



## **A Mathematical Model for the Dynamics of Large Membrane Deformations of Isolated Fibroblasts**

A. STÉPHANOU\*

The SIMBIOS Centre,  
Department of Mathematics,  
University of Dundee,  
Dundee DD1 4HN,  
Scotland

Lab. TIMC-IMAG, Equipe DynaCell,  
UMR CNRS 5525,  
Institut Albert Bonniot,  
38706 La Tronche Cedex,  
France

M. A. J. CHAPLAIN

The SIMBIOS Centre,  
Department of Mathematics,  
University of Dundee,  
Dundee DD1 4HN,  
Scotland

P. TRACQUI

Lab. TIMC-IMAG, Equipe DynaCell,  
UMR CNRS 5525,  
Institut Albert Bonniot,  
38706 La Tronche Cedex,  
France

In this paper we develop and extend a previous model of cell deformations, initially proposed to describe the dynamical behaviour of round-shaped cells such as keratinocytes or leukocytes, in order to take into account cell pseudopodial dynamics with large amplitude membrane deformations such as those observed in fibroblasts. Beyond the simulation (from a quantitative, parametrized model) of the experimentally observed oscillatory cell deformations, a final goal of this work is to underline that a set of common assumptions regarding intracellular actin dynamics and associated cell membrane local motion allows us to describe a wide variety of cell morphologies and protrusive activity.

The model proposed describes cell membrane deformations as a consequence of the endogenous cortical actin dynamics where the driving force for large-amplitude

---

\*Corresponding address: Institut de l'Ingénierie de l'Information de Santé, Faculté de Médecine  
Laboratoire TIMC, CNRS UMR 5525, Equipe Dynacell, 38706 La Tronche Cedex, France.  
*E-mail*: [astephan@netcourrier.com](mailto:astephan@netcourrier.com)

cell protrusion is provided by the coupling between F-actin polymerization and contractility of the cortical actomyosin network. Cell membrane movements then result of two competing forces acting on the membrane, namely an intracellular hydrostatic protrusive force counterbalanced by a retraction force exerted by the actin filaments of the cell cortex. Protrusion and retraction forces are moreover modulated by an additional membrane curvature stress.

As a first approximation, we start by considering a heterogeneous but stationary distribution of actin along the cell periphery in order to evaluate the possible morphologies that an individual cell might adopt. Then non-stationary actin distributions are considered. The simulated dynamic behaviour of this cytomechanical model not only reproduces the small amplitude rotating waves of deformations of round-shaped cells such as keratinocytes [as proposed in the original model of Alt and Tranquillo (1995, *J. Biol. Syst.* **3**, 905–916)] but is furthermore in very good agreement with the protrusive activity of cells such as fibroblasts, where large amplitude contracting/retracting pseudopods are more or less periodically extended in opposite directions. In addition, the biophysical and biochemical processes taken into account by the cytomechanical model are characterized by well-defined parameters which (for the majority) can be discussed with regard to experimental data obtained in various experimental situations.

© 2003 Society for Mathematical Biology. Published by Elsevier Ltd. All rights reserved.

## 1. INTRODUCTION

As repeatedly emphasised in the current literature, understanding cell motility (namely the ability of a cell to deform and migrate) and the mechanisms governing motility is a vital and essential task as it occurs in many important biological events such as embryogenesis, wound healing or the formation of primary solid tumours and metastases (secondary tumours). The fundamental challenge is to understand the complete scheme in which cell motion occurs in close relationship with the mechanisms of perception of the cell's extracellular medium (e.g., tissue) and the integration of the signals from the local environment. A cornerstone of this dynamic integration scheme is the spontaneous dynamic state of the cell, as revealed by the *in vitro* observations of cyclic changes of cell morphologies. In this context, one of the major propositions regarding cell behaviour, and the one on which this study is based, is the demonstration at the beginning of the 1990s of a certain self-organization of spontaneous cell deformation dynamics, which was until then widely considered as random. The existence of recurring patterns of deformation, such as the appearance of rotating waves of deformation around the cell body, was indeed demonstrated for various cell types such as keratinocytes (Alt *et al.*, 1995), leukocytes (Alt, 1990) and the dictyostelium amoebae (Killich *et al.*, 1993, 1994). These observations have driven the development of several theoretical models (Killich *et al.*, 1994; Alt and Tranquillo, 1995; Le Guyader and Hyver, 1997) which have tried to integrate molecular, chemical

and mechanical elements in order to determine and test the relative importance of the various elements and structure of the cell biophysical and biochemical processes responsible for this self-organization. The existence of what appears to be a 'spontaneous cell dynamic', where 'spontaneous' is taken in the sense of 'outwith any clearly identified and significant stimulations from the environment' (other than small amplitude environmental fluctuations), is a fundamental element to consider as it will affect the cell response to an external stimulation. Despite the relevance of the spontaneous cell dynamic, relatively few studies have been interested in this and remain, for the most part, focused on the migratory behaviour of cells. One reason for this is that the spatio-temporal analysis of cell deformations is a complicated and involved task, even if recent optical flow approaches avoid the need of cell contour segmentation [usually a limiting step for temporal analyses based on polarity maps (Stephanou *et al.*, 2003)]. It has now become clear that the extension/retraction motion of the cell membrane is directly related to the remodelling of the cytoskeleton and more particularly to the dynamic polymerization/depolymerization of actin (Condeelis, 1993; Carlier and Pantaloni, 1997; Borisy and Svitkina, 2000). Actin is a polymer which forms a dense and highly dynamic network of filaments located in the most flattened area found at the periphery (the cell cortex) of a cell cultured *in vitro* on a two-dimensional substrate.

Many different hypotheses have been proposed to explain how cell deformations occur and most of them have mainly focus on the mechanism of cell membrane extension or protrusion.

An early first hypothesis considered a sol/gel transition of actin regulated by local calcium concentration (Oster, 1984). Solation of actin is assumed to occur when a given threshold of calcium is reached. Solation thus triggers the expansion of the actin gel which pushes on the membrane. When the level/concentration of calcium falls below the threshold, re-gelation of actin occurs and the network is able to contract again. This hypothesis, however, requires the necessity of an initial ionic leak across the membrane in order to activate the solation/gelation process, which is therefore not spontaneous (self-consistent).

A second hypothesis suggests that actin polymerization in the neighbourhood of the membrane is the direct cause of protrusion (Theriot and Mitchison, 1991; Carlier and Pantaloni, 1997; Abraham *et al.*, 1999; Borisy and Svitkina, 2000). In this case, a Brownian ratchet mechanism has been proposed (Peskin *et al.*, 1993; Mogilner and Oster, 1996) to explain the intercalation of actin monomers (G-actin) between the growing end of actin filaments and the cell membrane. According to this mechanism, random thermal fluctuations, either of the cell membrane or of the actin fibres, are able to create the gap required for polymerization.

A third hypothesis proposes the involvement of certain molecular motors, with an active role for myosin I which, once coupled to the actin filaments, is able to propulse the filaments towards the membrane through various sliding mechanisms (Lee *et al.*, 1993; Small *et al.*, 1993).

However, the most often referred to hypothesis is the assumption of pressure-driven protrusion (Bereiter-Hahn and Luers, 1998). It is known that actin associated with myosin forms a contractile network. It is then assumed that the contraction of the network creates cytoplasmic flows throughout the cell which lead to an increasing pressure which is able to push the membrane outwards at any location where the membrane finds itself less strongly linked to the actin network. An alternative view proposes that the existence of a constant hydrostatic pressure is sufficient to produce the same effect (Alt and Tranquillo, 1995).

Our aim in this paper is to describe large membrane deformations as observed in resting fibroblasts cells. We thus use as a basis a cytomechanical model formulated initially proposed by Alt and Tranquillo (1995) which put forward the pressure-driven protrusion hypothesis.

The model assumes that the movements of the membrane depend on the interaction between an internal hydrostatic pressure pushing on the membrane and a counteracting stress due the actin filaments through their link with the membrane. The intensity of this retraction stress is assumed to be locally and linearly dependent on the local amount of actin available. Therefore the higher the actin density, the more the stress applied on the membrane is important. Moreover these two opposing forces are assumed to be modulated by an additional stress due to the membrane tension which depends on the intensity and sign of the local curvature of this membrane. As the cell deforms on a 2D substrate there is an additional friction stress characterizing the level of adhesiveness of the cell. Since actin is a polymer, the model obviously considers the actin polymerization kinetics regulated around a chemical equilibrium concentration. The contractile activity of the actomyosin complex (actin coupled to myosin) is also considered in the model. The actomyosin complex present in the cell cortex is described as a viscoelastic and contractile material linked to the membrane.

The model which describes the actin dynamics [by monitoring, for each instant, the actin density  $a(\theta, t)$  and its tangential velocity in the cell cortex  $v(\theta, t)$ ] in relation to the membrane extension width  $L(\theta, t)$  has been shown to be capable of simulating, in a very realistic way, rotating and pulsating deformations of cell membranes (Alt and Tranquillo, 1995; Stéphanou and Tracqui, 2002) such as those observed in keratinocytes and leukocytes (which are characterized, relatively speaking, by rounded shapes).

The above model, as it is conceived in its present formulation, remains restricted to being able to describe small membrane deformations such as those observed on certain types of cells where the width of the cell cortex  $L(\theta, t)$  remains small in front of the radius of the cell body  $R_0$  (see Fig. 1). Therefore, in this paper we would like to generalize this model and extend it in order to describe the dynamics of large membrane deformations, such as those observed on fibroblast cells (Fig. 2).

Indeed fibroblast cells present a different organization of their actin cytoskeleton, where actin filaments tend to form bundles which are radially oriented in the

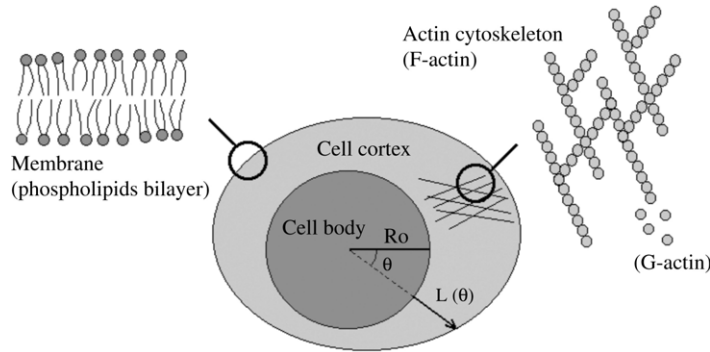


Figure 1. Schematic representation of the cell which illustrates the phospholipid bilayer, the cell membrane and the interconnected network of F-actin filaments which forms the actin cytoskeleton. The cell body is assumed to be confined in a circular area with radius  $R_0$ . The cell cortex where remodelling of the actin cytoskeleton mainly occurs corresponds to the area bounded at one side by the outer boundary of the cell body and at the other side by the cell membrane. The width of the cell cortex in any angular direction  $\theta$  is given by  $L(\theta)$ .

protrusive areas of the cell. These bundles stabilize the cell shape without depriving the cell of its motile abilities. Fibroblasts usually exhibit from 2 to 4 stable protrusions in the form of long and narrow membrane extensions homogeneously distributed around the cell body. In contrast to the deformations in round-shaped cells (mainly identified as rotating waves), the nature of the deformations observed in fibroblasts corresponds more to standing waves, where all the protrusions of the cell pulsate in a synchronized way according to various patterns. Despite their morphological and dynamical differences, it is commonly acknowledged that the same underlying mechanisms governing actin dynamics must apply.

In this paper, we first propose to investigate a very simple model for cell membrane movements inspired by the model of [Alt and Tranquillo \(1995\)](#). As we have noted the major limitation of Alt and Tranquillo's model is that it is only valid when dealing with small membrane extensions. This condition is imposed by the derivation of the curvature tension term. Our aim here is to propose a new derivation of that term in order to take into account large membrane extensions. For simplicity at this stage we will consider a time-invariant distribution of actin in the cell cortex, which is spatially varying in the tangential direction, i.e., along the cell cortex. We therefore consider static cell membrane deformations with the aim to evaluate the possible cell shapes that might thus be obtained and to estimate the influence of the new curvature tension term.

As a next step, we will restore the explicit coupling with the actin dynamics. For that, we will replace the (imposed) stationary spatial variation for F-actin concentration by self-generated variations induced by the coupling between F-actin polymerization and cell contractility controlled by the cortical actomyosin network (the latter depending non-linearly on the local amount of F-actin). We will then investigate how this coupling allows us to describe the various dynamical behaviours

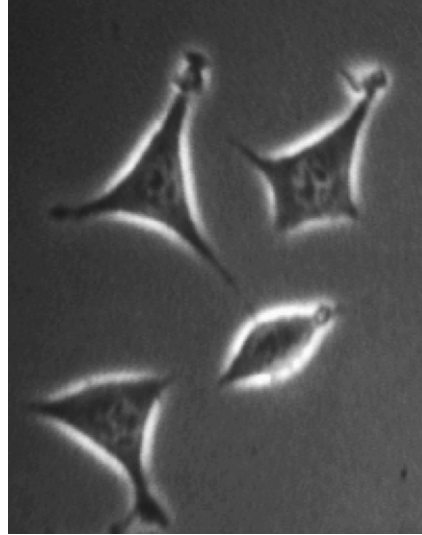


Figure 2. Videomicrograph of non-migrating L929 fibroblasts observed with phase contrast microscopy. This videomicrograph shows the most typical morphologies exhibited by this type of cell at their resting state (namely a non-migrating state). Fibroblasts typically present 'starry' morphologies involving from 2 to 4 thin membrane extensions which are more often homogeneously distributed around the cell body.

which exist, from rotating waves of deformations of round-shaped cells to large membrane extensions in the dynamical form of standing, pulsating waves (such as observed in fibroblasts).

A brief review for the characterization of the cell mechanical properties (more specifically the viscoelastic properties), will then be presented in order to provide a range of parameters from which a quantitative validation of the model will be discussed.

In the final section, we will present how the initial model of Alt and Tranquillo could be extended to deal with cell migration and how such an extension can be realized in the framework of our new model, in order to describe the main morphological features of fibroblast-type individual cell migration.

## 2. A MODEL FOR CELL MEMBRANE DEFORMATIONS

Experimentally, information on cell morphologies can be obtained from polarity maps (Killich *et al.*, 1993; Alt *et al.*, 1995; Stéphanou and Tracqui, 2002). These maps are obtained by extracting the coordinates of the points of the cell boundary and then reconstructing this boundary in a polar system of coordinates from the choice of a point of reference inside the cell as the origin of the polar coordinates. The point usually chosen as a reference point is the centre of the cell nucleus whose displacement in resting cells is very small in front of the cell membrane

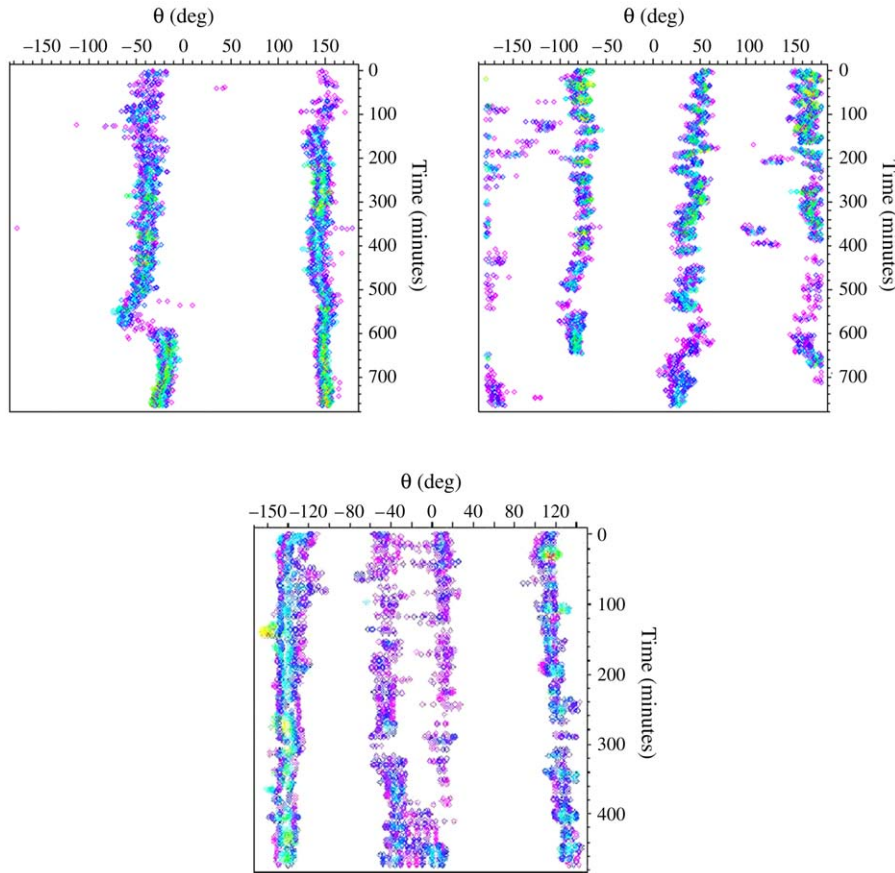


Figure 3. Spatio-temporal representations of the cells (cell polarity maps) which illustrates a variety of typical cell morphologies observed experimentally, with cells presenting, respectively, 2, 3 and 4 simultaneous protrusions each; the protrusive directions usually remain located along one axis for significantly long time periods (up to 12 h).

extensions. The polarity maps thus obtained for each instant are superposed with time to provide a spatio-temporal representation of the cell deformation dynamics. Fig. 3 presents a set of such spatio-temporal maps obtained from L929 fibroblasts and which exhibits typical cell morphologies of such resting cells. Fibroblasts exhibit from 2 to 4 stable protrusions. An example of each of these configurations is given in Fig. 3. One interesting feature of these cells is that the cell membrane protrusions are usually homogeneously distributed around the cell body, which gives symmetrical shapes. As we will see in what follows from our simulation results, spatio-temporal representations also provide an ideal tool to investigate cell membrane dynamics.

**2.1. The cytomechanical model.** The model we consider for the actin dynamics extends and develops an existing mechano-chemical model which describes an actin cytoskeleton (Lewis and Murray, 1991, 1992).

The model consists of two coupled equations, one describing the chemical dynamics of the material and the other describing its mechanical properties. We assume that the actomyosin network of our model retains the same mechanical properties as the actomyosin cytogel. The stress tensor thus consists of viscous  $\sigma_v$ , elastic  $\sigma_e$ , contractile  $\sigma_c$  and osmotic stress  $\sigma_p$  components. Whereas in the cytogel model sol/gel transition kinetics were considered, in our case we focus on the polymerization kinetics of actin as in the initial model of [Alt and Tranquillo \(1995\)](#). The system of equations describing the actin dynamics is thus written as:

$$\nabla \cdot (\sigma_v + \sigma_e + \sigma_c + \sigma_p) = 0, \quad (1)$$

$$\frac{\partial a}{\partial t} - D \Delta a + \nabla \cdot \left( a \frac{\partial \mathbf{u}}{\partial t} \right) = k_a (a_c - a), \quad (2)$$

where  $a$  represents the F-actin concentration,  $a_c$  the F-actin concentration at the chemical equilibrium which differentiates the states of polymerization and depolymerization whose rate of polymerization is controlled by the coefficient  $k_a$ ;  $D$  is the diffusion coefficient for F-actin;  $\mathbf{u} = (u, v)$  is a vector denoting the displacement of the elements of the actomyosin network from their original unstrained position, with  $u$  and  $v$  denoting the radial and tangential component respectively;  $\sigma_v, \sigma_e, \sigma_c, \sigma_p$  are the (viscous, elastic, contractile and pressure induced) stress tensors respectively given by

$$\sigma_v = \mu_1 \dot{\epsilon} + \mu_2 \dot{\phi} \mathbf{I}, \quad (3)$$

$$\sigma_e = E' [\epsilon + \nu' \phi \mathbf{I}], \quad (4)$$

$$\sigma_c = \sigma(a) \mathbf{I} = \psi a^2 e^{-a/a_{\text{sat}}} \mathbf{I}, \quad (5)$$

$$\sigma_p = -p(\phi) \mathbf{I} = \frac{P}{1 + \phi} \mathbf{I}, \quad (6)$$

where  $\epsilon = \frac{1}{2}(\nabla \mathbf{u} + \nabla \mathbf{u}^T)$  is the strain tensor,  $\mathbf{I}$  is the identity tensor,  $\phi = \nabla \cdot \mathbf{u}$  the dilation, and  $\mu_1$  and  $\mu_2$  are the shear and bulk viscosities of the actin network respectively. Finally  $E' = E/(1 + \nu)$  and  $\nu' = \nu/(1 - 2\nu)$  where  $E$  is the Young's modulus and  $\nu$  the Poisson's ratio. The function  $\sigma(a)$  represents the contractile activity of the actomyosin network. This function models the fact that the contractility increases according to a parabolic law with the actin concentration until a saturation concentration  $2a_{\text{sat}}$  from which an effect of compaction of the network occurs and leads the contractility to decrease exponentially.  $p(\phi)$  represents the osmotic stress which depends on the dilation  $\phi$ .

Membrane deformations are modelled on the basis of the equation proposed by [Alt and Tranquillo \(1995\)](#), but we consider here a new derivation of this equation in order to remove the constraint of small deformations imposed in the original derivation of this term. The mechanical forces acting on the cell membrane are:

- a constant protrusive force  $P$  due to the hydrostatic pressure existing inside the cell,
- an active force  $\sigma(a)$  which depends on the local concentration of actin,
- a membrane curvature-dependent force  $\tau K_L$ , where  $\tau$  is a constant coefficient characterizing the membrane tension,
- a friction force between the membrane and the substrate  $\Phi V = \Phi \partial L / \partial t$ , where  $\Phi$  is the friction coefficient characterizing the adhesiveness of the cell with the substrate.

Whereas in the model of [Alt and Tranquillo \(1995\)](#), a linear relation for the retraction force exerted by the network on the membrane was considered ( $\gamma La$ ), here we have replaced this linear dependency by the non-linear function  $\sigma(a)$ . This function thus models an active contraction of the network rather than a passive restoring force. The deformation of the membrane is thus given by

$$\Phi \frac{\partial L}{\partial t} = P - \sigma(a)L - \tau K_L \quad (7)$$

where  $L(\theta)$  denotes the radial extension of the cell cortex.

The full functional form of the membrane curvature  $K_L$  in polar coordinates and without any restriction to small deformations is given by the following expression (see [Appendix A](#)):

$$K_L = \frac{2\left(\frac{\partial L}{\partial \theta}\right)^2 - [L(\theta) + R_0]\frac{\partial^2 L}{\partial \theta^2} + [L(\theta) + R_0]^2}{\left[\left(\frac{\partial L}{\partial \theta}\right)^2 + [L(\theta) + R_0]^2\right]^{\frac{3}{2}}}, \quad (8)$$

where  $R_0$  represents the radius of the cell body ([Fig. 1](#)).

In the initial model of [Alt and Tranquillo \(1995\)](#), the membrane curvature-induced force was depending on the amount of actin in order to represent the membrane-cortex force, here we chose to consider a pure curvature-induced force independent of the actin density.

**2.2. Model simplification.** In order to simplify the model equations, and more especially to avoid the problem of a free moving cell boundary, we propose to restrict the description of the actin dynamics in a one-dimensional circular active layer of radius  $r_*$ . Therefore we do not consider any radial movements of actin in the cell cortex but we assume tangential displacements which can lead to local increase or decrease in density on the circle (i.e., in the tangential direction  $\theta$ ) which affect the intensity of the retraction force. With such an approximation, the two components of the mechanical equilibrium equation can be reduced to a unique equation whose derivation in polar coordinates leads to the following expression (see [Appendix B](#) for details on the derivation):

$$\frac{\partial}{\partial \theta} \left[ \frac{\mu}{r_*} \frac{\partial v}{\partial \theta} + \frac{\hat{E}}{r_*} \frac{\partial v}{\partial \theta} + \sigma(a) \right] = \frac{\alpha v}{2 r_*}, \quad (9)$$

where

$$\mu = \mu_1 + \mu_2, \quad \hat{E} = E'(1 + v'), \quad \text{and} \quad \alpha = E' \left[ 1 - \frac{\frac{3}{2} + v'}{\frac{3}{2} + \frac{\mu_2}{\mu_1}} \right].$$

In this paper we will restrict our study of the model equations by assuming that the parameter  $\alpha$  (which represents a viscoelastic coefficient) is always positive (details for the justification of this choice can be found in the [Appendix C](#)). This reasonable hypothesis thus assumes that  $v' < \frac{\mu_2}{\mu_1}$ . Membrane and actin network dynamics are coupled by means of the following equation, adapted from equation (2) and which describes the conservation of the amount of actin,  $Q(\theta, t) = L(\theta, t)a(\theta, t)$ , where  $Q(\theta, t)$  represents the peripheral actin mass distribution inside the cell cortex, distributed along the cell periphery:

$$\frac{\partial Q}{\partial t} - \frac{D}{r_*^2} \frac{\partial^2 Q}{\partial \theta^2} + \frac{1}{r_*} \frac{\partial}{\partial \theta} (Q\dot{v}) = k_a(Q_c - Q) \quad (10)$$

with  $Q_c(\theta, t) = L(\theta, t)a_c$ .

The equation for the membrane deformations is still given by

$$\Phi \frac{\partial L}{\partial t} = P - \sigma(a)L - \tau K_L. \quad (11)$$

### 3. NONDIMENSIONALIZATION AND LINEAR STABILITY ANALYSIS

**3.1. Nondimensionalization.** We nondimensionalize the equations by making the following substitutions:

$$\begin{aligned} \tilde{t} &= tk_a, & \tilde{a} &= \frac{a}{a_c}, & \tilde{L} &= \frac{L}{R_0}, & \tilde{v} &= \frac{\dot{v}}{k_a R_0}, & \tilde{D} &= \frac{D}{k_a R_0^2}, \\ \tilde{E} &= \frac{\hat{E}}{k_a \mu}, & \tilde{P} &= \frac{P}{k_a R_0 \Phi}, & \tilde{\tau} &= \frac{\tau}{k_a R_0^2 \Phi}, & \tilde{\alpha} &= \frac{\alpha}{k_a \mu}, \\ \tilde{\psi} &= \frac{\psi a_c^2}{k_a \mu}, & \tilde{a}_{\text{sat}} &= \frac{a_{\text{sat}}}{a_c}, \end{aligned}$$

where  $R_0$  represents a typical length in the cell, and  $\mu$  and  $\Phi$  are assumed to be equivalent coefficients. Dropping the tildes for notational convenience, the equations are written as:

$$\frac{\partial}{\partial \theta} \left[ \frac{1}{r_*} \frac{\partial \dot{v}}{\partial \theta} + \frac{E}{r_*} \frac{\partial v}{\partial \theta} + \sigma(a) \right] = \frac{\alpha}{2} \frac{v}{r_*}, \quad (12)$$

$$\frac{\partial}{\partial t} (La) - \frac{D}{r_*^2} \frac{\partial^2}{\partial \theta^2} (La) + \frac{1}{r_*} \frac{\partial}{\partial \theta} (La\dot{v}) = L(1 - a), \quad (13)$$

$$\frac{\partial L}{\partial t} = P - \sigma(a)L - \tau K_L \quad (14)$$

with

$$\sigma(a) = \psi a^2 e^{-a/a_{\text{sat}}}.$$

**3.2. Linear stability analysis.** The linear stability analysis is performed in order to define the conditions required for the model parameters to generate self-sustained oscillations of the membrane corresponding to the destabilization of the uniform steady state for the variable  $L$ , occurring through a Hopf bifurcation ( $\text{Re}[\lambda(k)] = 0$ ). The steady state is given by

$$a_0 = 1, \quad L_0 = \frac{P}{\sigma(1)}, \quad v_0 = 0. \tag{15}$$

All the equations are linearized about this steady state. The solutions of the linearized system are proportional to  $e^{\lambda t + ik\theta}$ . By substitution of this expression in the linearized equations we obtain the system

$$\begin{pmatrix} \lambda + \sigma(1) & L_0\sigma'(1) & 0 \\ \lambda + \frac{D}{r_*^2}k^2 & L_0(\lambda + \frac{D}{r_*^2}k^2 + 1) & ik\frac{L_0}{r_*}\lambda \\ 0 & ikr_*\sigma'(1) & -(\lambda + \Omega)k^2 - \frac{\alpha}{2} \end{pmatrix} \begin{pmatrix} L - L_0 \\ a - a_0 \\ v - v_0 \end{pmatrix} = \vec{0}, \tag{16}$$

with  $\Omega = E$  and  $\sigma'(1) = \partial\sigma(a)/\partial a|_{a=1}$ . The dispersion equation associated with this system is given by  $\det(M) = 0$  (where  $M$  is the matrix above), i.e.:

$$k^2\lambda^3 + a(k^2)\lambda^2 + b(k^2)\lambda + c(k^2) = 0, \tag{17}$$

where

$$\begin{aligned} a(k^2) &= \frac{D}{r_*^2}k^4 + [\Omega + 1 + \sigma(1) - 2\sigma'(1)]k^2 + \frac{\alpha}{2}, \\ b(k^2) &= \frac{D}{r_*^2}[\Omega + \sigma(1) - \sigma'(1)]k^4 \\ &\quad + \left[ \frac{\alpha D}{2 r_*^2} + \Omega(1 + \sigma(1) - \sigma'(1)) + \sigma(1)(1 - \sigma'(1)) \right] k^2 \\ &\quad + \frac{\alpha}{2}[1 + \sigma(1) - \sigma'(1)], \\ c(k^2) &= \frac{D}{r_*^2}\Omega[\sigma(1) - \sigma'(1)]k^4 + \left[ \frac{\alpha D}{2 r_*^2}(\sigma(1) - \sigma'(1)) + \sigma(1)\Omega \right] k^2 + \frac{\alpha}{2}\sigma(1). \end{aligned}$$

According to the Routh–Hurwitz criteria the condition for the roots of the dispersion equation to have a negative real part ( $\text{Re}(\lambda) < 0$ ) is

$$a(k^2) > 0, \quad c(k^2) > 0 \quad \text{and} \quad a(k^2)b(k^2) - c(k^2) > 0. \tag{18}$$

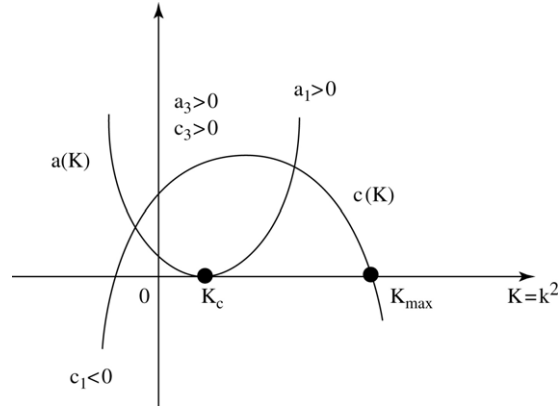


Figure 4. Conditions required to satisfy the Routh–Hurwitz criteria.

For simplicity, we represent the functions  $a(k^2)$ ,  $b(k^2)$  and  $c(k^2)$  by

$$\begin{aligned} a(k^2) &= a_1 k^4 + a_2 k^2 + a_3 \\ b(k^2) &= b_1 k^4 + b_2 k^2 + b_3 \\ c(k^2) &= c_1 k^4 + c_2 k^2 + c_3 \end{aligned}$$

and we have  $a_1 > 0$ ,  $a_3 > 0$ ,  $c_3 > 0$  and  $c_1 < 0$ .  $a_2$ ,  $b_1$ ,  $b_2$ ,  $b_3$  and  $c_2$  are not well defined, i.e., they can be either positive or negative. As  $c_1$  is negative, this means that the number of wavenumbers  $k$  for which  $c(k^2)$  is positive, is limited, i.e.,  $c(k^2) > 0$  only for  $k^2 \in [0, k_{\max}^2]$ . As  $a(k^2)$  is required to be positive at least for  $k^2 < k_{\max}^2$ , this means that  $b(k^2)$  must also be positive to fulfil the condition  $a(k^2)b(k^2) - c(k^2) > 0$ .

**3.3. Conditions for a bifurcation.** The stability analysis is thus performed as follows: first we determined the value of  $k_{\max}^2$  for the condition  $c(k^2) > 0$ , then as  $a_1$  and  $a_3$  are positive but  $a_2$  can be negative, this means that a bifurcation occurs when  $a(k_c^2) = 0$  (see Fig. 4). The wavenumber  $k_c^2$  is the point for which the function  $a(k^2)$  has its minimum at 0. We then have to make sure that the function  $b(k^2)$  remains positive for  $k^2 < k_{\max}^2$  according to the conditions obtained for the choice of the parameters. Details of each of these calculation steps are given in the Appendix C. The expressions obtained for  $k_{\max}^2$  and  $k_c^2$  are as follows:

$$k_{\max}^2 = \frac{2\sigma(1)}{\frac{D}{r_*^2}[\sigma'(1) - \sigma(1)]}, \tag{19}$$

$$k_c^2 = \frac{2\sigma'(1) - \sigma(1) - \Omega - 1}{2\frac{D}{r_*^2}} > 0. \tag{20}$$

Moreover the condition that the parameters must obey at the bifurcation point is given by

$$2\sigma'(1) - \sigma(1) - \Omega - 1 = \frac{\sqrt{2\alpha D}}{r_*}. \quad (21)$$

#### 4. MECHANICAL CHARACTERIZATION OF THE CELL

The model we chose to investigate is based on a mechanical (rather than molecular) description of the cell. Therefore, before we go further in the presentation and analysis of the simulation performed on the model, we present here a brief review of the experimental methods used to mechanically characterize the cell. This stage is essential for defining the range of parameters required for our simulation and at a later stage for the quantitative validation of the model. The mechanical characterization of the cell essentially consists in the determination of the viscoelastic properties of the cytoplasm (and the network of filaments) and the determination of the membrane elastic properties. Two different types of characterization methods can be distinguished: active methods and passive methods.

The first ‘active methods’ are methods where the determination of the viscoelastic parameters requires a direct mechanical interaction with the cell. Such mechanical interactions are usually performed with a micropipette (measurements of aspiration force) (Merkel *et al.*, 2000), microplates (deformations applied on the cell at varying frequencies) (Thoumine and Ott, 1997), or optical (Bar-Ziv *et al.*, 1998; Yanai *et al.*, 1999) and magnetic (Bausch *et al.*, 1998, 1999; Alenghat *et al.*, 2000) tweezers (mechanical stress applied in specific locations in the cell). The atomic force microscopy (Rotsch *et al.*, 1999; Rotsch and Radmacher, 2000) is another active method widely used, which consists in force mapping, i.e., recording force curves by scanning the sample cell with the tip of the device, from which local elastic moduli are measured.

Passive methods, on the other hand, are non-invasive for the cell, which gives them an advantage since the results obtained are far less method dependent than the active ones. Laser tracking micro-rheology (Xu *et al.*, 1998; Yamada *et al.*, 2000) for example, is a method used to estimate the mechanical properties of the cell by tracking the Brownian motion of individual particles naturally present in the cytoplasm of the cell. A closely related techniques is the diffusive wave spectroscopy. Rather than monitoring a single particle, this method monitors the relative motion of many thousands of particles simultaneously. In both methods the viscoelastic moduli are then evaluated from the motions of the particles. Scanning acoustic microscopy (Zoller *et al.*, 1997; Bereiter-Hahn and Luers, 1998) is another passive method which allows one to characterize the stiffness of a material from the reflection of sound waves. This is based on the measurement of the velocity of longitudinal sound waves which is proportional to the elasticity and density of the structure under observation. High sound velocity means high tension in

Table 1. Viscoelastic parameters from extracellular measurements or whole cell measurements.

Technique (Ref)	Cell type	Elasticity (N m <sup>-2</sup> )	Viscosity (N s m <sup>-2</sup> )
Magnetic twist (Zaner and Valberg, 1989)	Macrophage	n.a.	2500
Magnetic twist (Wang <i>et al.</i> , 1993)	Endothelial	2	n.a.
Magnetic twist (Pourati <i>et al.</i> , 1998)	Endothelial	10–12.5	n.a.
Magnetic twist (Laurent <i>et al.</i> , 2002, 2003)	Epithelial	34–85	5–14
Micropipette (Sung <i>et al.</i> , 1988)	Leucocyte	0.75 23.8	33
Mech. rheometer (Eichinger <i>et al.</i> , 1996)	<i>Dictyostelium</i>	55	25
Micropipette (Merkel <i>et al.</i> , 2000)	<i>Dictyostelium</i>	200 ± 10 (front)	
Micropipette (Merkel <i>et al.</i> , 2000)		330 ± 20 (rear)	
Cell poker (Zahalak <i>et al.</i> , 1990)	Neutrophil	118	n.a.
AFM (Radmacher <i>et al.</i> , 1996)	Platelet	100–5000	n.a.
Microplates (Thoumine and Ott, 1997)	Fibroblast	1000	100–10000
Spont. retraction (Ragsdale <i>et al.</i> , 1997)	Fibroblast	1700	4 × 10 <sup>5</sup>
Magnetic tweezers (Bausch <i>et al.</i> , 1998)	Fibroblast	30000	2000
Deformable substrat (Dembo and Wang, 1999)	Fibroblast	2000	n.a.
Deformable substrat (Dembo and Wang, 1999)		6000 (front)	n.a.

fibrillar elements of the cytoskeleton. The use of deformable substrates is another non-invasive technique which allows one to measure traction stresses exerted by migrating cells through the deformations they create on a flexible substrate. This approach can yield direct quantitative information about the detailed magnitude, direction and location of interfacial stresses. Wrinkles created by the cell tractions at the surface of the film are interpreted as the result of compressive forces exerted by migrating fibroblasts (Harris *et al.*, 1980). Other methods, however, use non-wrinkling silicon rubber film, and measure instead the displacement of polystyrene latex beads embedded in the film (Oliver *et al.*, 1999). Computational techniques are then used to convert the displacement information into an image of the traction stress distribution (Dembo *et al.*, 1996; Dembo and Wang, 1999).

**4.1. Mechanical parameters.** The results obtained from the various methods of characterization are summarized and completed by other measurements in order to provide a ‘global’ source of reference of the cell mechanical parameters presented in Tables 1–4.

## 5. SIMULATION RESULTS

**5.1. Static membrane deformations.** Before we perform the analysis of the full model, we first focus in this section on the equation governing the membrane deformations [equation (11)]. Our aim is to evaluate the ability of the simple membrane model to account for typical ‘steady-state’ deformations of fibroblast cells, such

Table 2. Viscoelastic parameters from intracellular measurements.

Technique (Ref)	Cell type	Elasticity (N m <sup>-2</sup> )	Viscosity (N s m <sup>-2</sup> )
Magnetic twist (Valberg and Albertini, 1985)	Macrophage	15	2000
Magnetic tweezers (Bausch <i>et al.</i> , 1999)	Macrophage	20–735	210
Optical tweezers (Yanai <i>et al.</i> , 1999)	Neutrophil	1.1 (body)	0.35
Optical tweezers (Yanai <i>et al.</i> , 1999)		0.01 (front)	0.1
Optical tweezers (Yanai <i>et al.</i> , 1999)		0.75 (rear)	0.35
Laser tracking (Yamada <i>et al.</i> , 2000)	Epithelial	72.1	38.2

Table 3. Traction force measurements.

Technique (Ref)	Cell type	Traction force (nN)
Deformable substrate (Oliver <i>et al.</i> , 1995)	Keratocyte	45 (ventral)
Deformable substrate (Oliver <i>et al.</i> , 1995)	Keratocyte	10
Micromachined (Galbraith and Sheetz, 1999)	Keratocyte	13 (max.)
Micromachined (Galbraith and Sheetz, 1999)		4.5 (ventral)
Micromachined (Galbraith and Sheetz, 1999)		0.158 (dorsal)
Deformable substrate (Burton <i>et al.</i> , 1999)	Keratocyte	100–200 (rear)
Deformable substrate (Burton <i>et al.</i> , 1999)		600–700 (body)
Deformable substrate (Burton <i>et al.</i> , 1999)		120–150 (flank)
Deformable substrate (Burton <i>et al.</i> , 1999)	Fibroblast	300–800
Deformable substrate (Dembo and Wang, 1999)	Fibroblast	2000
Microplate (Thoumine and Ott, 1997)	Fibroblast	40
Magnetic tweezers (Bausch <i>et al.</i> , 1999)	Macrophage	0.05–0.9
Magnetic tweezers (Guilford <i>et al.</i> , 1995)	Macrophage	2–10
Micropipette aspiration (Merkel <i>et al.</i> , 2000)	<i>Dictyostelium</i>	13 (retraction)

as exhibited in Fig. 2. For this, we replace here the retraction force  $\sigma(a)$  by the function  $\gamma(\theta)$  modulated along the angular position  $\theta$  (see Fig. 1) and that we used to reflect a static state of the actin distribution. The membrane movements are thus described by

$$\Phi \frac{\partial L}{\partial t} = P - \gamma(\theta)L - \tau K_L. \quad (22)$$

The function for the retraction force  $\gamma(\theta)$  is then given by

$$\gamma(\theta) = \gamma_0[\alpha + \sin(m\theta)]$$

where  $\alpha$  and  $m$  represent the coefficients which control the amplitude of the deformation and the mode of deformation respectively.

The analytical solution of equation (11), for the parameter  $\tau = 0$  (i.e., no membrane tension) and for an initial condition  $L(t = 0) = L_0$  (i.e., a circular shape), is given by

$$L(\theta, t) = \frac{P}{\gamma(\theta)} + \left( L_0 - \frac{P}{\gamma(\theta)} \right) e^{-\frac{\gamma(\theta)}{\Phi} t}. \quad (23)$$

Table 4. Membrane tension ( $k_B$  is the Boltzman's constant).

Parameter (Ref)	Value
Membrane tension (Simson <i>et al.</i> , 1998)	$3.1 \pm 1.4 \mu\text{N m}^{-1}$
Membrane tension (Cevc and Marsh, 1987)	$35 \mu\text{N m}^{-1}$
Membrane tension (Raucher and Sheetz, 2000)	$7.0 \pm 0.5 \text{ pN}$
Bending modulus (Simson <i>et al.</i> , 1998)	$391 \pm 156 k_B T$
Bending modulus (Cevc and Marsh, 1987)	$5\text{--}50 k_B T$
Adhesion energy (Simson <i>et al.</i> , 1998)	$22.0 \pm 12.2 \times 10^6 \text{ J m}^{-2}$

Table 5. Maximum and minimum extension of the membrane depending on the membrane tension coefficient  $\tau$ .

$\tau$	$L_{\min}$	$L_{\max}$	$\Delta L_{\max}$
0	0.40	2	1.60
0.05	0.41	1.63	1.21
0.1	0.43	1.42	0.99

The asymptotic solutions of this equation are presented in Fig. 5 (external curves in each case) for a range of modes from  $m = 1$  (round-shaped cell) to  $m = 10$  ('starry' shape). Fibroblasts usually display from 2 to 4 stable protrusions (Fig. 2). Although morphologies with more than four protrusions exist, they are more rarely observed as they are unstable. In each case the minimum and maximum deformation of the membrane, for the asymptotic state, is given by the following range:

$$\frac{P}{\gamma_0(\alpha + 1)} \leq L(\theta) \leq \frac{P}{\gamma_0(\alpha - 1)}. \quad (24)$$

The maximum amplitude of deformation  $\Delta L_{\max}$  is thus

$$\Delta L_{\max} = \frac{2P}{\gamma_0(\alpha + 1)(\alpha - 1)}. \quad (25)$$

In order to evaluate the influence of the curvature term on these morphologies, equation (11) is now solved for two different values of the membrane tension coefficient  $\tau$  (Table 5). The exact analytic resolution of this equation is this time non-trivial, and therefore the equation is solved numerically using a central finite difference scheme which leads to a tridiagonal matrix system solved by the Thomas algorithm (Strikverda, 1989).

The two solutions (for  $\tau = 0.05$  and  $\tau = 0.1$ ) calculated for each mode of cell deformation appear for each case in Fig. 5 as the two internal curves. We observe that the initial cell morphologies (those corresponding to  $\tau = 0$ ) are smoothed by the additional membrane tension term. As this term depends linearly on the intensity of the curvature, the more the curvature is sharp (such as in mode  $m = 5$  and  $m = 10$ ) the more the effect becomes important in smoothing the cell shapes.

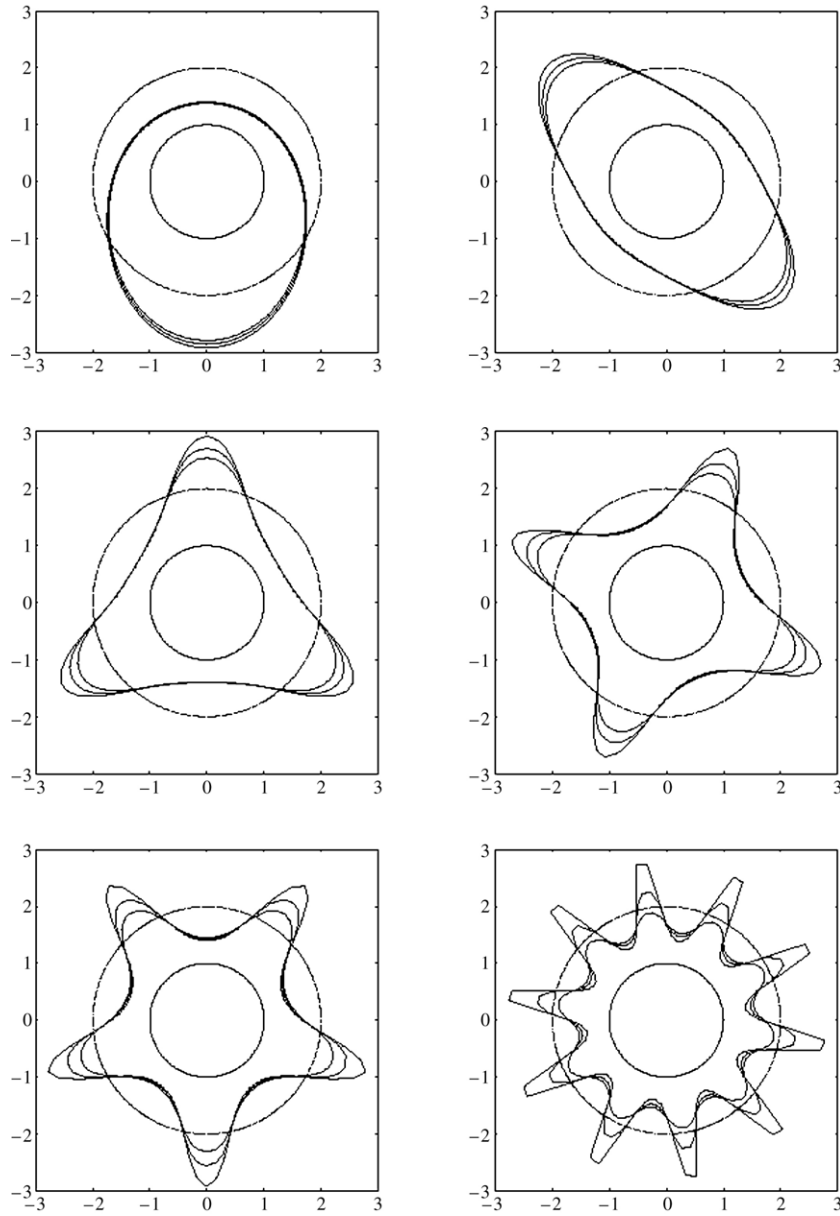


Figure 5. Potential cell morphologies obtained for various modes of deformation ( $m = 1, 2, 3, 4, 5, 10$ ) of the function  $\gamma(\theta)$  representing a spatial modulation of the F-actin filament stiffness. In each graph, the dotted curve represents the initial cell shape [circular shape  $L(\theta, t = 0) = L_0$ ] and the most external curve the analytical solution of the equation for the membrane deformations [equation (11)] taken for  $\tau = 0$  (passive membrane). The two internal curves correspond to the numerical solutions of that same equation for two different values of the membrane stiffness coefficient, namely  $\tau = 0.05$  and  $\tau = 0.1$ .

**5.2. The dynamical model.** In this section, we restore the explicit coupling between the membrane and the actin dynamics which is responsible for its

Table 6. Parameters of the simulations.

Figures	$D$	$\tau$	$\alpha$	$\psi$	$a_{\text{sat}}$	$P$	$E$
6(a)–6(b)	0.134	0	22	9	1.1	4	2
6(c)–6(d)	0.075	0	39	8	1.1	4	2
6(e)–6(f)	0.00962	0.1	304	10	1.1	4	2

movements. We thus solve now the full system of PDEs involving a hyperbolic [equation (10)], a parabolic [equation (11)] and an elliptic [equation (9)] equation. The hyperbolic and parabolic equations are evolution equations we solved numerically using a Crank–Nicholson finite differences scheme with appropriate discretisation. The elliptic equation is solved through a relaxation scheme. The associated matrix inversions were solved using the Thomas algorithm (Strikverda, 1989) adapted to incorporate the periodic boundary conditions. In all the simulations, the initial conditions are random perturbations of the F-actin concentration around the homogeneous steady-state where the cell has a circular morphology.

The results of the simulations carried out are presented in Fig. 6. In each case, the spatio-temporal maps for the membrane extension  $L(\theta, t)$  are displayed together with the associated actin distributions  $a(\theta, t)$ . The parameters used for each of the simulations are given in Table 6. Parameters,  $\tau$ ,  $a_{\text{sat}}$ ,  $\psi$ ,  $p$ ,  $P$  and  $E$  are arbitrarily defined.  $D$  is calculated from equation (20) for a given mode of deformation  $k_c$ . The parameter  $\alpha$  is then calculated from equation (21). The condition which imposes that  $b(k^2)$  is a positive function for the selected set of parameters is verified *a posteriori* (see Appendix C for details on the stability analysis).

In the first simulation (Fig. 6, top graphs) the parameters have been chosen in order to select a lower mode of deformation corresponding to round-shaped cells. We observe, after an oscillating transition phase (from  $t = 2$  to  $t = 10$  normalized time units), the slow emergence of a rotating wave of deformation around the cell body. The sequence of the asymptotic dynamical state of the cell membrane deformations is displayed in Fig. 7. The wave of deformation rotates in a counter-clockwise direction with a measured periodicity of about  $T = 2.8$  normalized time units. This dynamical behaviour is typical of round-shaped cells such as keratinocytes and leukocytes.

In the second simulation (Fig. 6, middle graphs), a symmetrical pulsating state rapidly emerges. The pulsation is characterized by the extension of the membrane along one direction and its simultaneous retraction in the other perpendicular direction. The associated sequence of deformations is displayed in Fig. 8. This time the periodicity of the pulsation is shorter with  $T = 2.2$  normalized time units. This pulsating behaviour is characteristic of fibroblast cells.

For the third simulation (Fig. 6, bottom graph) the parameters were defined according to the stability analysis of the previous section so that higher modes of deformation would be selected. The sequence showing the associated cell

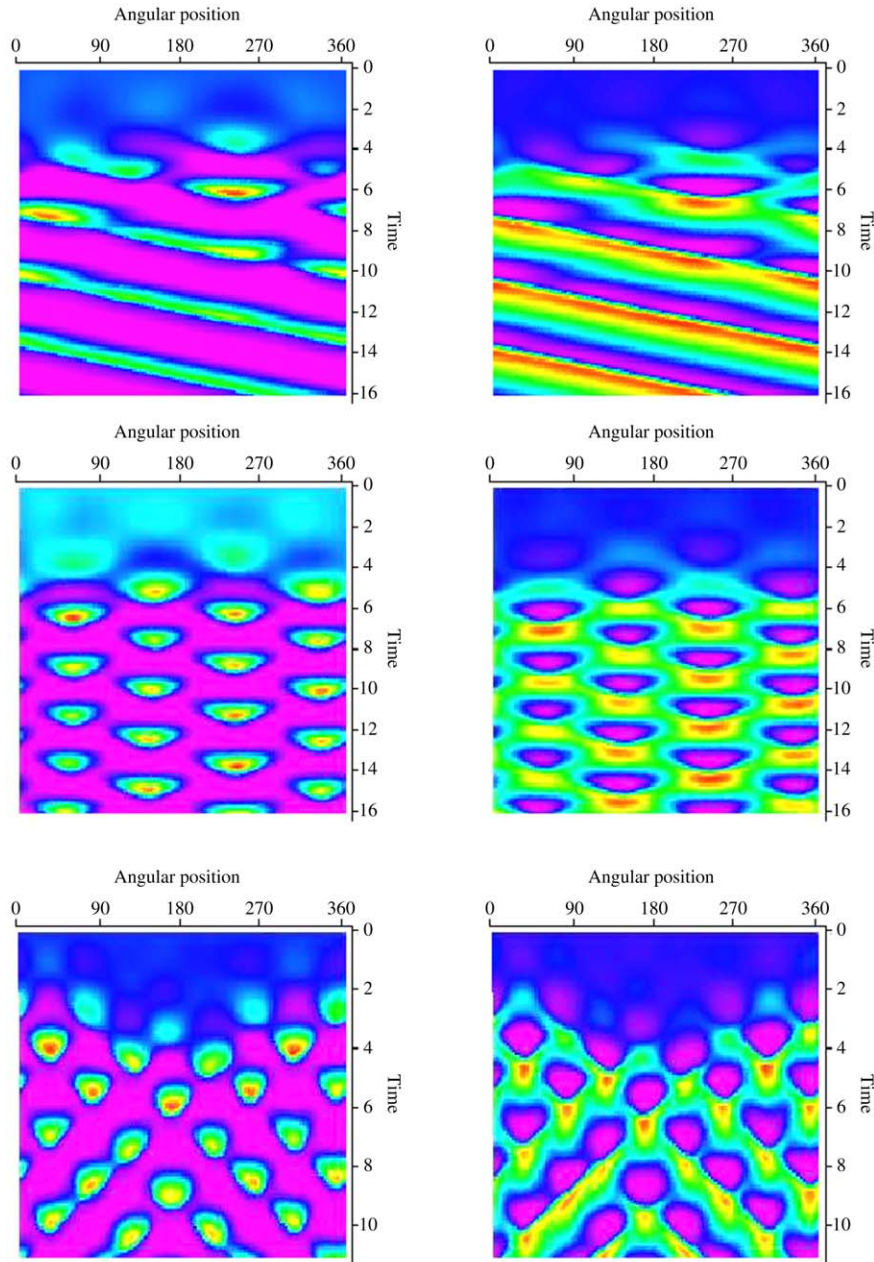


Figure 6. Simulation results of the spatio-temporal evolution of the cell membrane deformations (left side), together with the corresponding actin distributions (right side). Top graphs: rotating wave of deformation; middle graphs: symmetrical pulsation, bottom graphs: asymmetrical (or alternating) pulsation.

movements is displayed in Fig. 9. Snapshots of the simulated cell are taken to cover a full period of deformations where  $T = 2.8$  normalized time units, as for the rotating wave case. The simulated cell exhibits coordinated movements

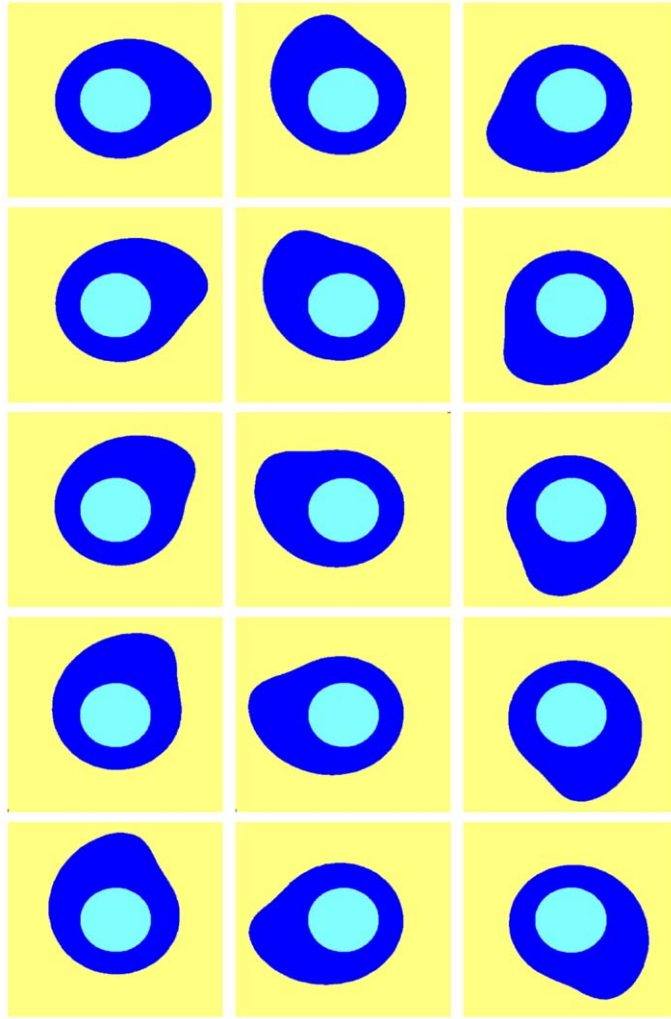


Figure 7. Simulated cell membrane deformations (asymptotic state associated with the top graph of Fig. 6). Snapshots are taken every 200 iterations ( $\Delta t = 0.2$ ). The counterclockwise wave of deformation has a periodicity of about 2.8 normalized time units (sequence to be read from top to bottom).

of extension/retraction of the membrane involving up to four protrusions simultaneously which occur in perpendicular directions from each other. This simulated dynamics of cell deformations is consistent with the movements observed in fibroblasts. A typical example of fibroblast deformations is shown in the videomicroscopy sequence presented in Fig. 10.

In the simulated sequence we observe that a developing protrusion presents a wide front (under the effect of the pressure) whereas during the retraction process the pseudopods become thinner (the actomyosin network pulls on the membrane). Experimentally this difference is not as obvious. However the developing

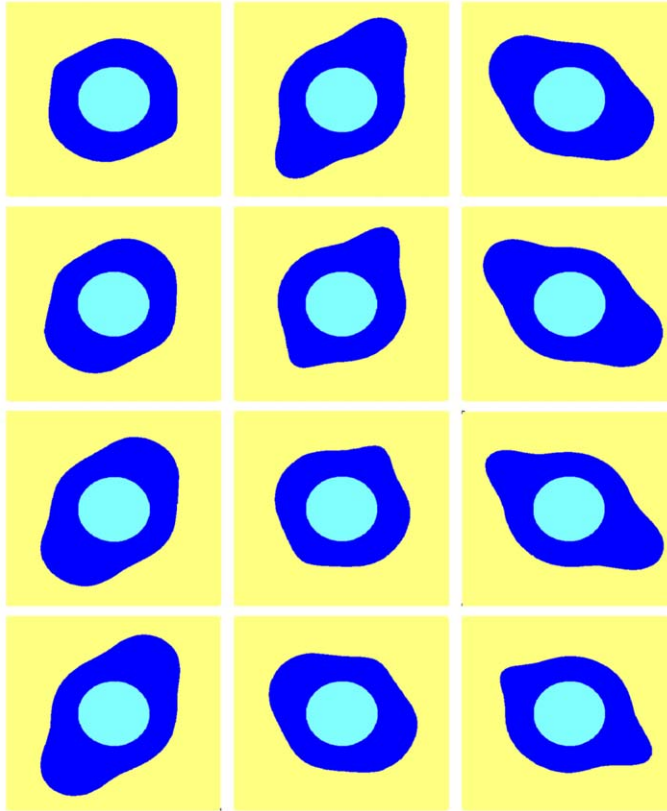


Figure 8. Simulated cell membrane deformations (asymptotical state associated with the middle graph of Fig. 6). Snapshots are taken every 200 iterations ( $\Delta t = 0.2$ ). The pulsation of the cell deformation has a periodicity of about 2.2 normalized time units (sequence to be read from top to bottom).

protrusions exhibit at their tips some kind of ‘blobs’ which disappear as soon as the pseudopods start to retract.

For a more detailed analysis, Fig. 11 simultaneously follows the evolution of the actin distribution as well as its tangential displacement. The 4 graphs presented correspond respectively to the snapshots 1, 3, 4 and 5 of Fig. 9 (associated simulation times are  $t = 5; 5.4; 5.6$  and  $5.8$  normalized units). In the protrusive areas (or pseudopods) the actin density is low and starts to polymerize (and reversely depolymerize in the areas where the critical density is reached,  $a_c = 1$ ). Simultaneously, tangential displacements of actin are observed from zones of low density to zones of higher density which tend to the homogenization of the actin distribution in the cell (Fig. 11, upper left graph). Actin progressively increases at the neighbourhood of the pseudopods. The intensification of the retraction force thus leads to the narrowing of the protrusions (Fig. 11, upper right graph). The actin then enters almost instantaneously in the remaining pseudopods (Fig. 11, bottom left graph) and the distributions of actin in the cell are reversed.

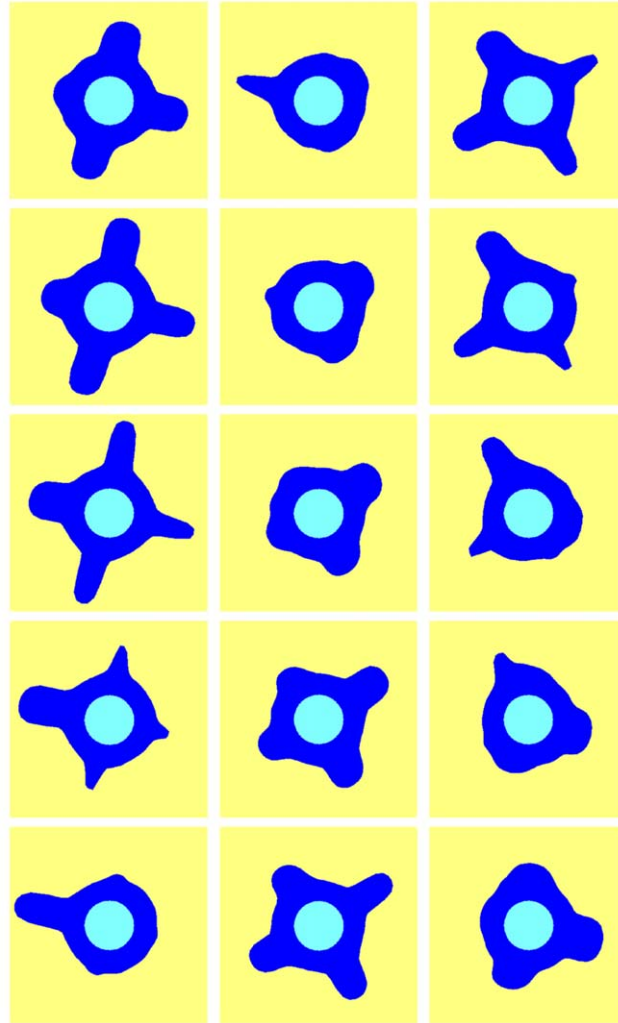


Figure 9. Simulated cell membrane deformations (asymptotic state associated with the bottom graph of Fig. 6). Snapshots are taken every 200 iterations ( $\Delta t = 0.2$ ). The alternating pulsation of the cell deformation has a periodicity of about 2.8 normalized time units (sequence to be read from top to bottom).

The retraction at the tips of the pseudopods is thus suddenly increased and leads to their total retraction (Fig. 11, bottom right graph). New pseudopods then appear in zones of low actin density and a new cycle can start.

Fig. 12 shows the oscillating dynamics on a longer time scale (up to  $t = 20$  normalized time units). The upper graph shows the simultaneous evolution of the amplitude of the cell membrane deformation associated with the actin concentration for a given direction corresponding to a pseudopod, and the lower graph shows the simultaneous evolution of the amplitude of two protrusive directions distant from each other with a  $45^\circ$  angle. Oscillations of the cell shape are exhibited with alternated directions of deformation from one cycle to the next one.

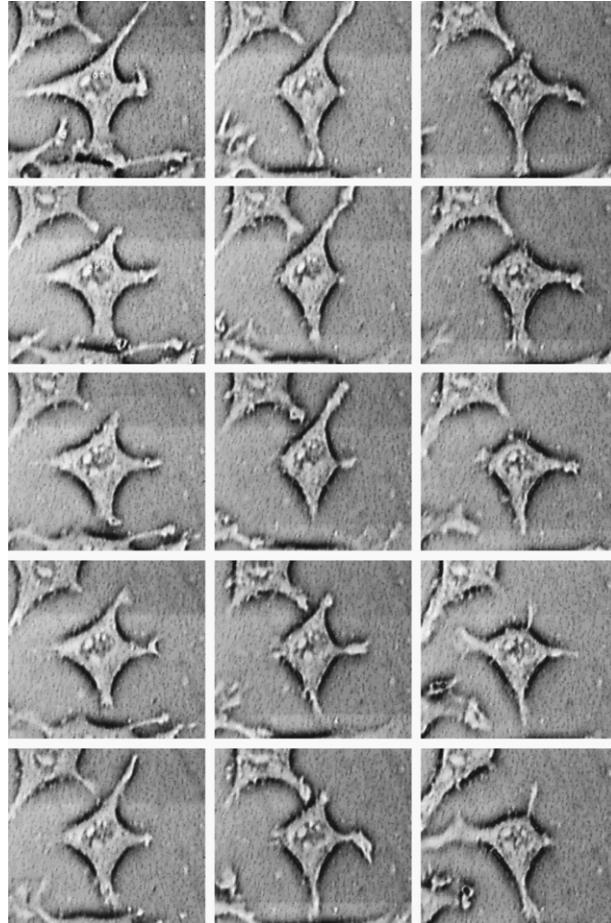


Figure 10. Videomicroscopy sequence of a L929 pulsating fibroblast. The time interval between two consecutive pictures is about 2 min (sequence to be read from top to bottom).

In the simulations performed, it has been possible to switch from one dynamical behaviour to another by changing mainly two key parameters, the diffusion coefficient  $D$  for actin in the cytoplasm and the coefficient  $\alpha$  which characterizes the cell viscoelastic properties [see equation (9)]. According to the normalization of the parameters (see Section 4.1), this last parameter can be evaluated from the values of  $k_a$  and  $\mu$  which are respectively the actin polymerization rate and the cytoplasmic viscosity, as follows:

$$\alpha = k_a \mu \tilde{\alpha} > 0. \quad (26)$$

The polymerization rate  $k_a$  can be estimated as

$$k_a = \frac{T_{\text{simul}}}{T_{\text{real}}} \quad (27)$$

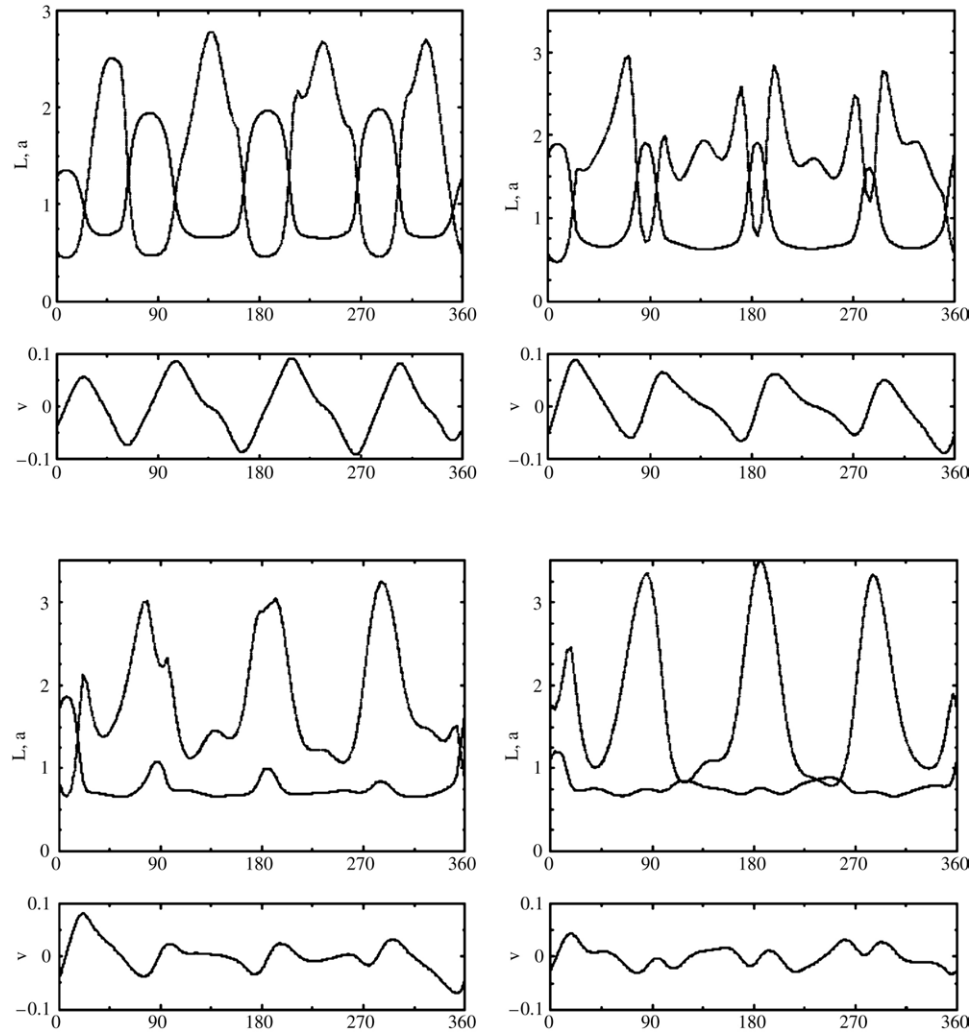


Figure 11. Simultaneous plots of actin distribution and corresponding membrane deformations in upper graphs. In the lower rectangular graphs, the associated tangential displacements of actin are displayed. These four graphs correspond to the snapshots 1, 3, 4 and 5 of the sequence of Fig. 7 associated with the normalized times 5, 5.4, 5.6 and 5.8 respectively.

where  $T_{\text{simul}}$  is the adimensional periodicity of the simulated cell deformations and  $T_{\text{real}}$  is the periodicity of the deformations measured on real cells. Then  $k_a$  has the dimension of 1/time i.e.,  $s^{-1}$ . This periodicity can be measured by the extraction of temporal signals for each protrusive direction detected on the experimental polarity maps (Fig. 3). Previous work with this method has allowed us to establish an existing periodicity for L929 fibroblasts of about 30 min (Stéphanou *et al.*, 2003).

Concerning the cytoplasmic viscosity  $\mu$ , the experimental data collected in Tables 1 and 2 obtained from different studies and using different techniques, lead

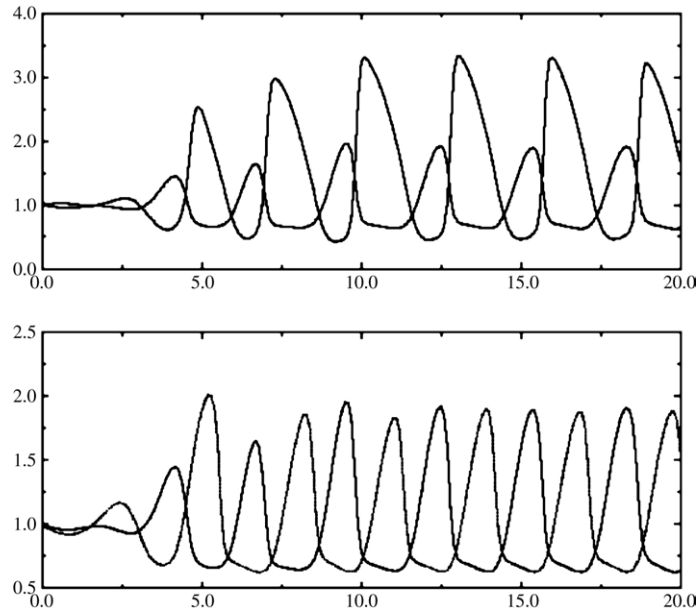


Figure 12. Upper graph: evolution over time of the cell membrane deformations and of the associated actin distribution (higher amplitude curve) in normalized units, for a given protrusive direction. Lower graph: simultaneous evolution of the membrane deformations for two protrusive directions at  $45^\circ$  from each other.

Table 7. Estimated cell elasticity.

Figure	$T_{\text{simul}}$	$\tilde{\alpha}$	$\alpha_{\text{estim}} (\text{N m}^{-2})$
6(a)–6(b)	2.8	22	68
6(c)–6(d)	2.2	39	95
6(e)–6(f)	2.8	304	945

us to take an estimated value around  $2000 \text{ N s m}^{-2}$  (Valberg and Albertini, 1985; Zaner and Valberg, 1989; Bausch *et al.*, 1998). On this basis, an estimated value of the  $\alpha$  coefficient can be obtained for each of the three simulations performed. The values calculated are display in Table 7.

In Tables 1 and 2, we observe that higher values of the cell elasticity are found for fibroblasts cells, namely cells with large deformation amplitudes, whereas smaller values are rather associated with rounded cells (such as endothelial cells, leukocytes or neutrophils). Similarly in our simulations, we managed to obtain fibroblast-type morphologies by increasing significantly the coefficient  $\alpha$ . This parameter is a complex one as it depends on the coefficients  $E'$ ,  $\nu'$ ,  $\mu_1$  and  $\mu_2$ . It can therefore be considered as a coefficient which reflects the global viscoelastic properties of the cell. We note that simulations performed with smaller values of this coefficient lead at the opposite to rounded-cell type deformation.

## 6. DISCUSSION AND CONCLUSION

A large variety of behaviour, from rotating waves of deformations to pulsating waves, have been observed, all in a single type of cell, the amoeba *Dictyostelium* (Killich *et al.*, 1993, 1994). A purely geometrical model based on the interaction of superposed waves was used to describe the dynamical behaviours observed. It was shown that the interference patterns of two interacting waves were sufficient to describe the overall diversity of the oscillating states observed in the amoebae. It was then proposed that actin dynamics might account for these oscillations. This affirmation has here been confirmed on the basis of the cytomechanical model initially formulated by Alt and Tranquillo (1995). We have indeed been able to simulate rotating waves of deformations for the selection of low modes of deformation associated with round-shaped cells such as keratinocytes, and to simulate standing pulsating waves of deformation for the selection of higher modes of deformations associated with star-shaped cell morphologies involving large membrane extensions such as for fibroblasts. In this latter case, the model is especially in good agreement with the experimentally observed cell dynamical behaviours as it is able to catch the main features of the fibroblast cells. This is achieved through a fine tuning of the two key concentrations for actin:—the concentration at the chemical equilibrium  $a_c$  which determines the polymerization and depolymerization state of actin and—the saturation concentration  $2a_{\text{sat}}$  which regulates the intensity of the retraction force.

Considering our relatively good agreement with experimental observations, the assumption that the actin redistribution essentially occurs in the tangential direction appears to be reasonable when dealing with fibroblast deformations. Indeed actin filaments in the cell are preferentially organized radially in the cortex and remain stable in that direction and thus tends to stabilize the cell shape (Cramer *et al.*, 1997). This stabilizing effect, probably linked to the development of new adhesion sites in coordination with the formation of bundles of filaments, is not taken into account by the model and leads to a very motile cell with protrusions occurring in many different spatial directions. However, our globally satisfactory simulation results tend to confirm the formulated mechano-chemical hypotheses, especially the controversial hypothesis of pressure-driven protrusion. They also tend to confirm the idea that the same basic mechanisms might apply and account for the all diversities of different cell behaviours (from rotating to standing waves) and their associated shapes (from round-shaped leukocytes to the large pseudopods of fibroblasts).

From now, a logical extension of the model would be to take into account cell migration in order to provide a complete model for (individual) cell motility.

Such a model extension has already been carried out on the basis of the initial model proposed by Alt and Tranquillo (1995). Realistic migratory behaviour of round-shaped cells (such as leukocytes) could be generated (Stephanou and Tracqui, 2002), but once again because of the limitation of the model which only deals

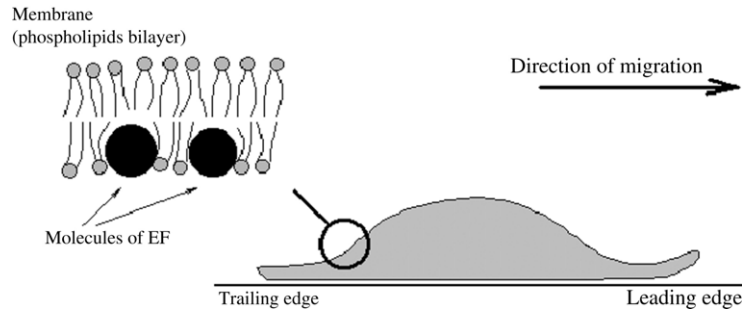


Figure 13. Schematic representation of a migrating cell exhibiting a characteristic dome-like shape where the thickest part represents the cell body. From the mechanical point of view, intercalation of molecules in the membrane is responsible for cell morphological instabilities.

with small membrane extensions, cell lamellipodial extension remained very small. However, now with our new model formulation, it becomes possible to generate fibroblast-type migration, which means to take into account the large lamellipodial extension, the salient feature of fibroblast migration preceding cell translocation.

In the case of chemotaxis, the cell responds to a gradient of chemoattractant diffusing in the medium. Therefore, in order to switch from the spontaneous pulsating state to the migrating state, the model has to incorporate the perception of an extracellular factor by the cell. Rather than consider a molecular point of view, which would involve the cascade of chemical events triggered by the molecules binding to the membrane and leading to actin polymerization and then cell migration, we have chosen to consider a mechanical point of view. This means that we do not consider the chemical properties of the chemoattractant molecules but instead their mechanical interactions with the cell membrane as solid objects (Fig. 13).

Indeed the presence of particle in the membrane leads to a release of the membrane tension as has been demonstrated in several studies (Kim *et al.*, 1998; Nielsen *et al.*, 1998; Soares and Maghelly, 1999). This effect is taken into account in the model by considering that the membrane tension coefficient  $\tau$  depends linearly on the local concentration  $C$  of the extracellular factor at the membrane, namely,

$$\tau(C) = \tau - \Lambda(C) \quad (28)$$

where  $\Lambda(C)$  is a function which characterizes the sensitivity of the cell to the extracellular factor. This function can be assumed to first increase with an increased concentration of factor and to decrease when a threshold concentration value is reached. This for example can model the fact that all the membrane receptors become saturated with the factor. However, for simplification, we assume here a linear dependency with the concentration i.e.,  $\Lambda(C) = \Lambda C$ , where the coefficient  $\Lambda$  is switched to 0, above the concentration threshold  $C_{\max}$ .

Therefore in the presence of an extracellular gradient of molecules, the membrane tension becomes weaker at the front of the cell (which faces the gradient)

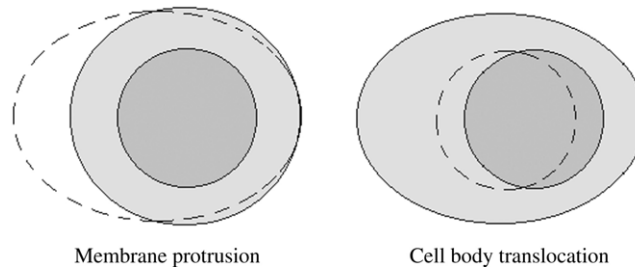


Figure 14. Schematic diagram exhibiting the two-step mechanism of migration, with first the membrane extension along the migration direction and second the cell body translocation, i.e., the displacement of the cell body at the new position of the cell geometrical barycentre. This second step occurs when the adhesion force becomes able to overcome the tension force of the actomyosin fibres in the cortex.

and allows a morphological instability to develop under the form of a lamellipodial extension. Assuming that the membrane receptors (e.g., integrins) are homogeneously distributed on the membrane, the developing lamellipod provides a bigger surface of contact of the cell with its substrate at the front than at its trailing edge. The adhesion force then becomes able to support the traction force exerted by the actomyosin complex whose contraction pulls the cell forward in a simplified two-step mechanism as displayed in Fig. 14 and which summarizes the five-step migration process described by Sheetz *et al.* (1999) i.e., (1) membrane extension, (2) attachment to the substrate, (3) cell contraction, (4) release of the attachment at the trailing edge and (5) recycling of the receptors.

Various simulations describing a range of experimental situations of cell migration have been performed from the extension of the initial model of Alt and Tranquillo (1995) (Stéphanou and Tracqui, 2002). In these simulations, a chemoattractant diffusing from a point source has been used. Here we show the results obtained for a front of chemoattractant. This corresponds to the case where the cell is initially very close to the source (see Fig. 15). The initial state is a circular cell which rapidly deforms by extending a lamellipod at the front. However in this case no real migration of the cell can be achieved as the limitation of small membrane extension imposed by the initial model formulation is reached. This simulation however suggests that large lamellipodial extension can be described and migration achieved from the new model.

Another perspective of this work would also be to further develop the model in order to take into account higher levels of actin organization such as the formation of bundles and the description of the inhomogeneous radial actin distribution in the cell cortex through a real two-dimensional formulation of the mechanochemical system of equations.

The ultimate aim of cell motility modelling would be to be able to propose a more complete and reliable model of cell movements which once dynamically calibrated by experimental data would help to drive new experiments by defining optimum conditions required in order to obtain a given cell behaviour. Knowing which

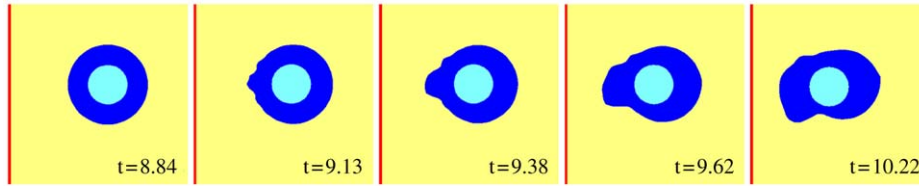


Figure 15. Migration of the cell towards a linear front of chemoattractant, which shows limited lamellipodial extension due to the small deformation limitation of the initial model.

parameters of the model to act on to achieve a desired behaviour (such as increasing the migration rate to favour wound healing or decreasing the migration rate to inhibit cell membrane deformations and migration and subsequently to prevent the invasive spread of cancer cells) would be a major achievement in the field of cell biology.

### ACKNOWLEDGEMENTS

The work of A. S. is funded by the Région Rhône-Alpes. We would like to thank Anne Doisy, Corinne Alcouffe and Xavier Ronot for providing the videomicrographs of cultured fibroblasts. We also thank the referees for valuable comments and suggestions on the paper.

### APPENDIX A: DERIVATION OF THE CURVATURE TERM IN THE MODEL

The expression for the curvature  $K$  in the 2D plan ( $R^2$ ) defined parametrically by  $C(s) = (x(s), y(s))$  is given by [Stoker \(1969\)](#)

$$K = \frac{x'y'' - x''y'}{(x'^2 + y'^2)^{\frac{3}{2}}}$$

where  $x' = \frac{dx}{ds}$ ,  $y' = \frac{dy}{ds}$ .

To determine the curvature in polar coordinates  $(r, \theta)$ , we apply the above formula to

$$\begin{cases} x = r(\theta) \cos \theta, \\ y = r(\theta) \sin \theta. \end{cases}$$

With  $r' = dr/d\theta$  and  $r'' = d^2r/d\theta^2$ , the expression of the curvature obtained for the polar system of coordinates  $(r, \theta)$  is given by

$$K = \frac{2r'^2 - rr'' + r^2}{(r'^2 + r^2)^{\frac{3}{2}}}.$$

We can thus deduce from this expression the curvature of the cell membrane in the geometry of our model where  $R_0$  is the internal radius of the cell delimiting

the cell body and  $L(\theta)$  the extension of the membrane taken from the surface of the cell body. The curvature is

$$K = \frac{2\left(\frac{\partial L}{\partial \theta}\right)^2 - (L(\theta) + R_0)\frac{\partial^2 L}{\partial \theta^2} + (L(\theta) + R_0)^2}{\left[\left(\frac{\partial L}{\partial \theta}\right)^2 + (L(\theta) + R_0)^2\right]^{\frac{3}{2}}}. \quad (\text{A.1})$$

## APPENDIX B: DERIVATION OF THE MECHANICAL EQUILIBRIUM EQUATION IN POLAR COORDINATES

The mechanical equilibrium equation is given by

$$\nabla \cdot [\mu_1 \dot{\epsilon} + \mu_2 \dot{\phi} I + E'(\epsilon + v' \phi I) + \sigma(a)I - p(\phi)I] = 0. \quad (\text{B.1})$$

For the sake of simplicity, we propose a 1D approximation where actin dynamics are restricted to the circle of radius  $r_*$ . No displacement of actin is allowed in the radial direction  $u$  and no contraction of the cytogel can occur in that direction. Therefore  $\frac{\partial a}{\partial r} = 0$ ,  $\frac{\partial u}{\partial r} = 0$ ,  $\frac{\partial v}{\partial r} = 0$  and  $u = 0$ . Although this is very schematic, this hypothesis leads to a qualitative agreement with experimental data. Of course, an explicit description of the structural links between the actin cytoskeleton and the membrane will require the consideration of a full 2D model derivation with both tangential and radial displacements.

The strain tensor in polar coordinates is thus given by

$$\epsilon = \begin{pmatrix} \frac{\partial u}{\partial r} & \frac{1}{2} \left( \frac{1}{r} \frac{\partial u}{\partial \theta} + \frac{\partial v}{\partial r} - \frac{v}{r} \right) \\ \frac{1}{2} \left( \frac{1}{r} \frac{\partial u}{\partial \theta} + \frac{\partial v}{\partial r} - \frac{v}{r} \right) & \frac{1}{r} \frac{\partial v}{\partial \theta} + \frac{u}{r} \end{pmatrix} = \begin{pmatrix} 0 & -\frac{v}{2r} \\ -\frac{v}{2r} & \phi \end{pmatrix},$$

with the dilation  $\phi = \nabla \cdot \mathbf{u} = \text{tr}(\epsilon) = \frac{\partial u}{\partial r} + \frac{1}{r} \frac{\partial v}{\partial \theta} + \frac{u}{r} = \frac{1}{r} \frac{\partial v}{\partial \theta}$ .

The condition for zero divergence of a stress tensor in polar coordinates is

$$\nabla \cdot \sigma_{\text{total}} = \begin{cases} \frac{\partial}{\partial r} \sigma_{rr} + \frac{1}{r} \frac{\partial}{\partial \theta} \sigma_{r\theta} + \frac{\sigma_{rr} - \sigma_{\theta\theta}}{r} = 0 \\ \left( \frac{\partial}{\partial r} + \frac{2}{r} \right) \sigma_{r\theta} + \frac{1}{r} \frac{\partial}{\partial \theta} \sigma_{\theta\theta} = 0. \end{cases}$$

We apply this formula to equation (1) of our model, where the total tensor is the sum of the individual viscous, elastic, contractile and pressure induced stress tensors given by the equations (3)–(6) respectively. The components of the global stress tensor  $\sigma$  are then given by

$$\begin{cases} \sigma_{rr} = \mu_2 \dot{\phi} + E' v' \phi + \sigma(a) - p(\phi) \\ \sigma_{r\theta} = -\frac{1}{2r} (\mu_1 \dot{v} + E' v) \\ \sigma_{\theta\theta} = (\mu_1 + \mu_2) \dot{\phi} + E' (1 + v') \phi + \sigma(a) - p(\phi) \\ \sigma_{rr} - \sigma_{\theta\theta} = -(\mu_1 \dot{\phi} + E' \phi). \end{cases}$$

The equations for the mechanical equilibrium in polar coordinates, with our conditions  $u = 0$  and  $\frac{\partial a}{\partial r} = 0, \frac{\partial u}{\partial r} = 0, \frac{\partial v}{\partial r} = 0$ , are thus:

$$\begin{aligned} (\frac{3}{2}\mu_1 + \mu_2)\dot{\phi} + E'(v' + \frac{3}{2})\phi &= -r\frac{\partial p(\Phi)}{\partial r}, \\ \frac{\partial}{\partial \theta}[(\mu_1 + \mu_2)\dot{\phi} + E'(1 + v')\phi + \sigma(a)] &= \frac{1}{2r_*}(\mu_1\dot{v} + E'v). \end{aligned}$$

Integration of the first equation  $p = 0$  gives the following expression for  $\dot{v}$ :

$$\dot{v} = -sv + C_0 \quad \text{with } s = \frac{E'(v' + \frac{3}{2})}{\frac{3}{2}\mu_1 + \mu_2}.$$

$C_0$  is a free constant, which is set to zero as actin displacement is null at the stationary state. Replacement of this expression in the second equation gives

$$\frac{\partial}{\partial \theta}[(\mu_1 + \mu_2)\dot{\phi} + E'(1 + v')\phi + \sigma(a)] = \frac{v}{2r_*}(E' - \mu_1s).$$

The resulting equation can thus be re-written as follows:

$$\frac{\partial}{\partial \theta}[\mu\dot{\phi} + \hat{E}\phi + \sigma(a)] = \frac{\alpha}{2} \frac{v}{r_*}, \tag{B.2}$$

or

$$\frac{\partial}{\partial \theta} \left[ \frac{\mu}{r_*} \frac{\partial \dot{v}}{\partial \theta} + \frac{\hat{E}}{r_*} \frac{\partial v}{\partial \theta} + \sigma(a) \right] = \frac{\alpha}{2} \frac{v}{r_*}, \tag{B.3}$$

with

$$\mu = \mu_1 + \mu_2, \quad \hat{E} = E'(1 + v'), \quad \alpha = E' - \mu_1s.$$

### APPENDIX C: LINEAR STABILITY ANALYSIS

(i) **Determination of  $k_{\max}^2$ .** As  $c_1$  is negative,  $c(k^2)$  can be positive only for a finite number of wave numbers  $k^2$ .  $c(0) = c_3$  being positive, the range of  $k^2$  for which the function  $c(k^2)$  is positive is thus given by  $k \in [0, k_{\max}^2]$ , where  $k_{\max}^2$  is solution of  $c(k^2) = 0$ , i.e.,

$$c_1k^4 + c_2k^2 + c_3 = 0, \quad \text{with the solution: } k_{\max}^2 = \frac{2\sigma(1)}{\frac{D}{r_*^2}[\sigma'(1) - \sigma(1)]}.$$

(ii) **Determining the conditions for a bifurcation.** As  $a_1$  and  $a_3$  are positive, a bifurcation occurs for the wavenumber  $k_c^2$  where  $a(k_c^2) = 0$ ,  $k_c^2$  being the

wavenumber for which the function  $a(k^2)$  is minimum, i.e.,

$$\frac{da(k_c^2)}{dk^2} = 2a_1k_c^2 + a_2 = 0 \quad \text{and} \quad k_c^2 = -\frac{a_2}{2a_1} > 0,$$

$$k_c^2 = \frac{2\sigma'(1) - \sigma(1) - \Omega - 1}{2\frac{D}{r_*^2}} > 0.$$

The condition for  $k_c^2$  to exist is that:  $2\sigma'(1) > \sigma(1) + \Omega + 1$ . The bifurcation occurs for  $a(k_c^2) = 0$ , and thus if we replace the expression found for  $k_c^2$  in this equation we obtain the condition that the parameters must obey at the bifurcation point, i.e.,:

$$2\sigma'(1) - \sigma(1) - \Omega - 1 = \frac{\sqrt{2\alpha D}}{r_*}. \tag{C.1}$$

Moreover, we must have  $k_c^2 < k_{\max}^2$ .

**Note:** We assume for the study of the equations of the model that the parameter  $\alpha$  is positive. However  $\alpha$  can obviously be also negative. If  $\alpha$  is negative then the coefficients  $c_3$  and  $a_3$  are negative. In that case, no bifurcation can be observed as the value of  $k^2$  for which  $a(k^2) = 0$  cannot correspond at the same time to the minimum point of the function. This means that the selection of a given unstable mode is this time not obvious. This justifies our choice to restrict our study to the case where  $\alpha$  is assumed to be positive.

**(iii) Verification that  $b(k^2)$  is positive.** The most favourable situation would be to have  $b(k^2) > 0$  for any  $k^2 \in [0, k_{\max}^2]$ . For such a situation,  $b_1$  and  $b_3$  must be positive. Therefore,

$$\begin{aligned} \text{if } b_1 > 0 & \quad \text{then } \Omega + \sigma(1) - \sigma'(1) > 0, \\ \text{if } b_3 > 0 & \quad \text{then } 1 + \sigma(1) - \sigma'(1) > 0, \\ \text{if } \Omega > 1 & \quad \text{then } b_3 > 0 \text{ therefore } b_1 > 0. \end{aligned}$$

Thus  $b(k^2) > 0$  for any  $k$  if the minimum of the function  $b(k^2)$  is positive, i.e.,

$$\frac{db(k_0^2)}{dk^2} = 0 \quad \text{and} \quad b(k_0^2) > 0 \text{ lead to } k_0^2 = -\frac{b_2}{2b_1} \text{ then } b_2 < 0.$$

So we have the condition

$$\frac{\alpha D}{2r_*^2} + \Omega[1 + \sigma(1) - \sigma'(1)] < \sigma(1)[1 - \sigma'(1)]. \tag{C.2}$$

The condition  $b(k^2) > 0$  is true if  $b(k_0^2) > 0$ , i.e.

$$b(k_0^2) = b_1k_0^4 + b_2k_0^2 + b_3 > 0 \quad \text{therefore we must have} \quad 4b_1b_3 > b_2^2.$$

## REFERENCES

- Abraham, V. C., V. Krishnamurthi, D. Lansing Taylor and F. Lanni (1999). The actin based nanomachine at the leading edge of migrating cells. *Biophys. J.* **77**, 1721–1732.
- Alenghat, F. J., B. Fabry, K. Y. Tsai, W. H. Goldmann and D. E. Ingber (2000). Analysis of cell mechanics in single vinculin-deficient cells using a magnetic tweezer. *Biochem. Biophys. Res. Commun.* **277**, 93–99.
- Alt, W. (1990). Mathematical models and analysing methods for the lamellipodial activity of leukocytes. *NATO ASI (Adv. Sci. Inst.) Ser. H, Cell Biol.* **42**, 407–422.
- Alt, W., O. Brosteanu, B. Hinz and W. H. Kaiser (1995). Patterns of spontaneous motility in videomicrographs of human epidermal keratinocytes. *Biochem. Cell. Biol.* **73**, 441–459.
- Alt, W. and R. T. Tranquillo (1995). Basic morphogenetic system modeling shape changes of migrating cells: how to explain fluctuating lamellipodial dynamics. *J. Biol. Syst.* **3**, 905–916.
- Bar-Ziv, R., E. Moses and P. Nelson (1998). Dynamic excitations in membranes induced by optical tweezers. *Biophys. J.* **75**, 294–320.
- Bausch, A. R., W. Moller and E. Sackmann (1999). Measurement of local viscoelasticity and forces in living cells by magnetic tweezers. *Biophys. J.* **76**, 573–579.
- Bausch, A. R., F. Ziemann, A. A. Boulbitch, K. Jacobson and E. Sackmann (1998). Local measurements of viscoelastic parameters of adherent cell surfaces by magnetic bead microrheometry. *Biophys. J.* **75**, 2038–2049.
- Bereiter-Hahn, J. and H. Luers (1998). Subcellular tension fields and mechanical resistance of the lamella front related to the direction of locomotion. *Cell. Biochem. Biophys.* **29**, 243–262.
- Borisy, G. G. and T. M. Svitkina (2000). Actin machinery: pushing the envelope. *Curr. Opin. Cell. Biol.* **12**, 104–112.
- Burton, K., J. H. Park and D. Lansing Taylor (1999). Keratocytes generate traction forces in two phases. *Mol. Biol. Cell* **10**, 3745–3769.
- Carlier, M. F. and D. Pantaloni (1997). Control of actin dynamics in cell motility. *J. Mol. Biol.* **269**, 459–467.
- Cevc, G. and D. Marsh (1987). *Phospholipid Bilayers*, New York: Wiley.
- Condeelis, J. (1993). Life at the leading edge: the formation of cell protrusions. *Annu. Rev. Cell. Biol.* **9**, 411–444.
- Cramer, L. P., M. Siebert and T. J. Mitchison (1997). Identification of novel graded polarity actin filaments bundles in locomoting heart fibroblasts: implications for the generation of motile force. *J. Cell. Biol.* **136**, 1287–1305.
- Dembo, M., T. Oliver, A. Ishihara and K. Jacobson (1996). Imaging the traction forces exerted by locomoting cells with the elastic substratum method. *Biophys. J.* **70**, 2008–2022.
- Dembo, M. and Y. L. Wang (1999). Stresses at the cell-to-substrate interface during locomotion of fibroblasts. *Biophys. J.* **76**, 2307–2316.
- Eichinger, L., B. Koppel, A. A. Noegel, M. Schleicher, M. Schliwa, K. Weijer, W. Witke and P. A. Janmey (1996). Mechanical perturbation elicits a phenotypic difference between Dictyostelium wild-type cells and cytoskeletal mutants. *Biophys. J.* **70**, 1054–1060.
- Galbraith, C. G. and M. P. Sheetz (1999). Keratocytes pull with similar forces on their dorsal and ventral surfaces. *J. Cell. Biol.* **147**, 1313–1323.
- Guilford, W. H., R. C. Lantz and R. W. Gore (1995). Locomotive forces produced by single leukocytes in vivo and in vitro. *Am. J. Physiol.* **268**, C1308–C1312.

- Le Guyader, H. and C. Hyver (1997). Periodic activity of the cortical cytoskeleton of the lymphoblast: modelling by a reaction-diffusion system. *C. R. Acad. Sci. Paris* **320**, 59–65.
- Harris, A., D. Stopak and P. Wild (1980). Silicon rubber substrata: a new wrinkle in the study of cell locomotion. *Science* **208**, 177–179.
- Killich, T., P. J. Plath, H. Bultmann, L. Rensing and M. G. Vicker (1993). The locomotion shape and pseudopodial dynamics of unstimulated dictyostelium cells are not random. *J. Cell. Sci.* **106**, 1005–1013.
- Killich, T., P. J. Plath, H. Bultmann, L. Rensing and M. G. Vicker (1994). Cell movement and shape are non-random and determined by intracellular, oscillatory rotating waves in dictyostelium amoebae. *Biosystems* **33**, 75–87.
- Kim, K. S., J. Neu and G. Oster (1998). Curvature-mediated interactions between membrane proteins. *Biophys. J.* **75**, 2274–2291.
- Laurent, V. M., S. Henon, E. Planus, R. Fodil, M. Balland, D. Isabey and F. Gallet (2002). Assessment of mechanical properties of adherent cells by bead micromanipulation: comparison of magnetic twisting cytometry vs optical tweezers. *J. Biomech. Eng.* **124**, 408–421.
- Laurent, V. M., E. Planus, R. Fodil and D. Isabey (2003). Mechanical assessment by magnetocytometry of the cytosolic and cortical cytoskeletal compartments in adherent epithelial cells. *Biorheology* **40**, 235–240.
- Lee, J., A. Ishihara and K. Jacobson (1993). How do cells move along surfaces? *Trends Cell. Biol.* **3**, 366–370.
- Lewis, M. A. and J. D. Murray (1991). Analysis of stable two-dimensional patterns in contractile cytogel. *J. Nonlinear Sci.* **1**, 289–311.
- Lewis, M. A. and J. D. Murray (1992). Analysis of dynamic and stationary pattern formation in the cell cortex. *J. Math. Biol.* **31**, 25–71.
- Merkel, R., R. Simson, D. A. Simson, M. Hohenadl, A. Boulbitch, E. Wallraff and E. Sackmann (2000). A micromechanic study of cell polarity and plasma membrane cell body coupling in Dictyostelium. *Biophys. J.* **79**, 707–719.
- Mogilner, A. and G. Oster (1996). The physics of lamellipodial protrusion. *Eur. Biophys. J.* **25**, 47–53.
- Nielsen, C., M. Goulian and O. S. Andersen (1998). Energetics of inclusion-induced bilayer deformations. *Biophys. J.* **74**, 1966–1983.
- Oliver, T., M. Dembo and K. Jacobson (1995). Traction forces in locomoting cells. *Cell. Motil. Cytoskeleton* **31**, 225–240.
- Oliver, T., M. Dembo and K. Jacobson (1999). Separation of propulsive and adhesive traction stresses in locomoting keratocytes. *J. Cell. Biol.* **145**, 589–604.
- Oster, G. F. (1984). On the crawling of cells. *J. Embryol. Exp. Morph. Supp.* **83**, 329–364.
- Peskin, C. S., G. M. Odell and G. F. Oster (1993). Cellular motions and thermal fluctuations: the Brownian ratchet. *Biophys. J.* **65**, 316–324.
- Pourati, J., A. Maniotis, D. Spiegel, J. L. Schaffer, J. P. Butler, J. J. Fredberg, D. E. Ingber, D. Stamenovic and N. Wang (1998). Is cytoskeletal tension a major determinant of cell deformability in adherent endothelial cells? *Am. J. Physiol. (Cell Physiol.)* **274**, C1283–C1289.
- Radmacher, M., M. Fritz, C. M. Kacher, J. P. Cleveland and P. K. Hansma (1996). Measuring the viscoelastic properties of human platelets with the atomic force microscope. *Biophys. J.* **70**, 556–567.

- Ragsdale, G., K. J. Phelps and K. Luby-Phelps (1997). Viscoelastic response of fibroblasts to tension transmitted through adherent junctions. *Biophys. J.* **73**, 2798–2808.
- Raucher, D. and M. P. Sheetz (2000). Cell spreading and lamellipodial extension is regulated by membrane tension. *J. Cell. Biol.* **148**, 127–136.
- Rotsch, C., K. Jacobson and M. Radmacher (1999). Dimensional and mechanical dynamics of active and stable edges in motile fibroblasts investigated by using atomic force microscopy. *Proc. Natl Acad. Sci.* **96**, 921–926.
- Rotsch, C. and M. Radmacher (2000). Drug-induced changes of cytoskeletal structure and mechanics in fibroblasts: an atomic force microscopy study. *Biophys. J.* **78**, 520–535.
- Sheetz, M. P., D. Felsenfeld, C. G. Galbraith and D. Choquet (1999). Cell migration as a five-step cycle. *Biochem. Soc. Symp.* **65**, 233–243.
- Simson, R., E. Wallraff, J. Faix, J. Niewohner, G. Gerisch and E. Sackmann (1998). Membrane bending modulus and adhesion energy of wild-type and mutant cells in *Dicystostelium* lacking talin or cortexillins. *Biophys. J.* **74**, 514–522.
- Small, J. V., A. Rohlfis and M. Herzog (1993). Actin and cell movement, in *Cell Behaviour: Adhesion and Motility*, G. Jones, C. Wigley and R. Warn (Eds), The Society of Experimental Biology, pp. 57–71.
- Soares, K. M. and C. C. Maghelly (1999). Linear instability analysis and mechanical interfacial tension. *J. Theor. Biol.* **196**, 169–179.
- Stephanou, A., X. Ronot and P. Tracqui (2003). Analysis of cell motility combining cytomechanical model simulations and an optical flow method, in *Polymer and Cell Dynamics—Multiscale Modelling and Numerical Simulation*, W. Alt, M. Chaplain, M. Griebel and J. Lenz (Eds), Basel: Birkhauser-Verlag, pp. 91–112.
- Stephanou, A. and P. Tracqui (2002). Cytomechanics of cell deformations and migration: from models to experiments. *C. R. Biol.* **325**, 295–308.
- Stoker, J. J. (1969). *Differential Geometry*, Wiley-Interscience.
- Strikverda, J. C. (1989). Finite difference schemes and partial differential equations, in *Wadsworth and Brooks/Cole*, Mathematics Series.
- Sung, K. L., P. C. Dong, G. W. Schmidt-Schonbein, S. Chien and R. Skalak (1988). Leukocyte relaxation properties. *Biophys. J.* **54**, 331–336.
- Theriot, J. A. and T. J. Mitchison (1991). Actin microfilament dynamics in locomoting cells. *Nature* **352**, 126–131.
- Thoumine, O. and A. Ott (1997). Time scale dependent viscoelastic and contractile regimes in fibroblasts probed by microplate manipulation. *J. Cell. Sci.* **110**, 2109–2116.
- Valberg, P. A. and D. F. Albertini (1985). Cytoplasmic motions, rheology and structure probed by a novel magnetic particle method. *J. Cell Biol.* **101**, 130–140.
- Wang, N., J. P. Butler and D. E. Ingber (1993). Mechanotransduction across the cell surface and through the cytoskeleton. *Science* **260**, 1124–1127.
- Xu, J., A. Palmer and D. Wirtz (1998). Rheology and microrheology of semiflexible polymer solutions: actin filament networks. *Macromolecules* **31**, 6486–6492.
- Yamada, S., D. Wirtz and S. C. Kuo (2000). Mechanics of living cells measured by laser tracking microrheology. *Biophys. J.* **78**, 1736–1747.
- Yanai, M., J. P. Butler, T. Suzuki, A. Kanda, M. Kurachi, H. Tashiro and H. Sasaki (1999). Intracellular elasticity and viscosity in the body, leading and trailing regions of locomoting neutrophils. *Am. J. Physiol. (Cell Physiol.)* **277**, C432–C440.
- Zahalak, G. I., W. B. McConnaughey and E. L. Elson (1990). Determination of cellular mechanical properties by cell poking, with an application to leukocytes. *J. Biomech. Eng.* **112**, 283–294.

- Zaner, K. S. and P. A. Valberg (1989). Viscoelasticity of F-actin measured with magnetic microparticles. *J. Cell Biol.* **109**, 2233–2243.
- Zoller, J., K. Brandle and J. Bereiter-Hahn (1997). Cellular motility in vitro as revealed by scanning acoustic microscopy depends on cell–cell contacts. *Cell Tissue Res.* **290**, 43–50.

*Received 24 October 2002 and accepted 17 November 2003*